Title
THE ENHANCEMENT OF SUBSTRUCTURE STRENGTHENING OF MARTENSITE

Author
Cheng, I-lin.

Publication Date
1970-05-01

UCRL-19196

c. 2

THE ENHANCEMENT OF SUBSTRUCTURE STRENGTHENING OF MARTENSITE

I-lin Cheng
(Ph. D. Thesis)

May 1970

AEC Contract No. W-7405-eng-48

LAWRENCE RADIATION LABORATORY
UNIVERSITY of CALIFORNIA BERKELEY

UCRL-19196

Cy 2

DISCLAIMER

Contents

THE ENHANCEMENT OF SUBSTRUCTURE STRENGTHENING OF MARTENSITE

I-lin Cheng

Inorganic Materials Research Division, Lawrence Radiation Laboratory
Department of Materials Science and Engineering, College of Engineering,
University of California, Berkeley, California

ABSTRACT

The structure and mechanical properties of two types of precipitation hardenable austenite alloys are studied. One is based on Fe-22Ni-4Mo-0.28C where the precipitates are Mo_2C and the other is Fe-28Ni-2Ti where the precipitates are coherent FCC γ' (Ni_3Ti) ordered phase.

Both types of alloy can be transformed martensitically in liquid nitrogen, thus rendering possible the study of the effect of precipitates on the substructures of martensite and the kinetics of martensitic transformation. It is found that the substructure strengthening effect of martensite could be enhanced by dispersion hardening the austenite prior to martensitic transformation.

In addition, the stabilities of the austenitic alloys are such that (1) upon certain aging treatments, the alloys transform partially to martensite (due to precipitation of solute atoms), thus the mechanical properties of these "composite" materials could be evaluated in terms of the strengthening effect of each of the component phases. (2) Upon straining, martensite forms in both types of alloys and microstructure observations are then made.

I. INTRODUCTION

Ausforming is a thermomechanical treatment, whereby the metastable austenite is deformed at elevated temperatures before isothermal decomposition takes place and then cooled to allow the martensite transformation to occur. The mechanical properties of ausformed martensite are in general superior to those of conventional heat treated martensite, for example, the tensile strength could be increased by as much as 30% with generally an improvement in ductility.

It has been concluded previously[1,2,3] that the high strength of ausformed martensite is controlled primarily by the high dislocation density in the structure. More recent work[4] showed that strengthening was achieved by the formation of subgrains (or cell structures) as well as the increased dislocation density in martensite as a result of ausforming.

However, the strength levels attained by prior austenitic deformation for alloys with essentially no carbon, e.g., maraging type alloys,[5] or steels having no strong carbide forming elements (Mo, Cr, V, etc) e.g., low alloy 4340 steel,[6] are not greatly increased; that is, a poor ausforming response in terms of improved properties. Hence, it is known that carbon and carbide forming elements are indispensible to obtain a useful ausforming response.[1-7] It has also been shown that carbides are formed during deformation of metastable austenite, either directly detected by electron microscope[1] or indirectly deduced from the increase in Ms temperature.[8] The role of these carbides was thought to pin the dislocation substructures in austenite so that the latter are not likely to be swept away by the advancing martensite boundaries on subsequent martensitic transformation and are thus inherited in the resulting structure. In addition, the carbides can also result in

the generation and multiplication of dislocations generated during the γ-α' phase transformation. The resulting substructures high density dislocation in ausformed martensite is then produced from either prior deformation or shear transformation and possibly both.

The major difficulty in the extensive application of ausformed steels is the large amount of plastic deformation required in order to cause appreciable strengthening in the resulting martensite as compared with the conventional heat treated martensites, for example, even H-11 alloyed steel, a high ausforming response steel, has a strength increase of about 1000 ~ 1300 psi per percent reduction deformation.[9,10]

It is the purpose of this thesis to investigate the significant strengthening contribution(s) and hence the origins of the high dislocation density in ausformed martensite. Generally, the martensitic transformation can be considered as a special kind of plastic deformation, where the thermodynamic driving force is analogous to the applied stress. Also, a very much higher work hardening rate of the alloys containing a second phase particle was observed, which was presumably due to an increase in dislocation density.

Hence, if we dispersion harden the austenite and take maximum advantage of the martensitic shear transformation, e.g., enhance the substructure strengthening effect by the presence of particles, etc., it may be expected that the strength attained in this way should not differ too much from that of normal ausformed steels. That is, the process of deforming austenite is just to introduce the necessary carbide to effect pinning and multiplication as pointed out by Thomas.[1] Consequently, the ausforming process could possibly be replaced by a process of dispersion-hardening the austenite followed by quenching to martensite.

Two types of alloys were used in this research. The first one was based on an alloy of Fe-22Ni-4Mo-0.28C. The choice of Mo as an alloying element is due to its highest diffusivity as compared to the other carbide formers [1] (hence greatest strengthening contribution and rapid kinetics of precipitation). This alloy was then deformed in the austenitic condition and subsequently recovered or recrystallized in an attempt to reduce the dislocation density but retain the carbides. The "recovered" austenite was then quenched to martensite and compared with the normal ausformed martensite. The second type was an Fe-28Ni-2Ti alloy, where proper aging in austenitic condition (ausaging) was known to produce the precipitation of γ' (Ni_3Ti) particles.[11] The microstructure and mechanical properties of the martensite quenched from ausaged specimens were then analysed in order to help understand the role played by precipitates or particles during the martensitic transformation.

In addition, there were two "by-products" as a result of this investigation. The first one was the formation of strain-induced martensite upon straining the metastable austenite; in other words, the stabilities of the austenite in both types of alloys were such that plastic deformation between Ms and Md temperatures yields martensite. The production of strain induced martensite during plastic deformation is well known[12] to increase the work hardening rate and delay premature necking. Therefore, a combination of high strength, ductility and toughness was possible and was actually the essence of the development of the so-called "TRIP" steels.[13] The second "by-product" was the formation of a mixture of austenite and martensite upon suitable aging treatment. This phenomenon was again related to the stability of austenite. Since Ms temperature was

shown experimentally[14] to be depressed by nearly all alloying elements except Co, the depletion of solute atoms from the matrix by precipitation should generally raise the Ms temperature. Consequently, martensite should form partially after cooling to room temperature. The resulting mixed-phase structure would provide an interesting aspect. Work done on 304 stainless steel[15] has shown that the yield strength of a "composite" of martensite and austenite was linearly proportional to the amount of martensite regardless of what kind of treatment was performed to form it. In the present case, because both the martensitic and austenitic phases were strengthened substructurally, e.g., by dislocations and precipitates, what was, then, the effect of these strengthening parameters (work hardening, precipitation hardening, etc.) on the overall yield strength behavior of the "composite" as a function of the amount of martensite?

Finally, it should be mentioned that this investigation entailed a correlation between the substructure and mechanical properties whenever possible. The former was examined primarily by transmission electron microscopy.

II. EXPERIMENTAL PROCEDURES

A. Material

Two types of alloy containing Mo and Ti respectively were used in this study. For the sake of convenience, the Mo containing alloy is assigned as Type I alloy and the Ti alloy as Type II. Table I lists their chemical compositions. Type II alloy was kindly supplied by International Nickel Company through Dr. J. R. Mihalisin.

TABLE I Chemical Composition of Alloys (Wt.%)

	Fe	Ni	Mo	Ti	C
Type I	bal	21.67	4.11	----	0.24
Type II	bal	27.69	----	2.01	0.005

B. Thermal and Mechanical Treatments

(1) Type I alloy:

The ingot was cast in a vacuum melting furnace. It was homogenized first at 1250°C for three days and rolled to 0.125" thick blank after reheating to 1000°C. The rolled sheets were then annealed at 1200°C for two hours, put in a 500°C furnace and reduced 30% in thickness immediately. The products were water-quenched after rolling. Tensile test sheet specimens and coupons for measuring Ms temperatures, x-ray diffraction and transmission electron and optical microscopy were machined from the ausformed sheets.

The samples were vacuum-sealed in quartz tubes for subsequent annealing treatments at temperatures of 500°C and 600°C respectively. Martensitic structures were obtained by quenching the annealed specimens into liquid nitrogen.

(2) Type II alloy:

The materials were received as hot-rolled sheets of about 80 mils in thickness, from which tensile test specimens and coupons were machined. The samples were then solution heat treated in argon atmosphere at 1100°C for two hours followed by rapid water quenching. It should be noted here that a high quenching rate was very important, as, otherwise, the Ms temperature could be raised above room temperature due to the precipitation of Ni_3Ti. Aging treatments were performed at 300°C, 500°C, and 600°C for various periods of time. Subzero temperature cooling was performed by liquid nitrogen (LN) and a mixture of liquid nitrogen and methyl alcohol (LNA) at about -100°C.

C. Mechanical Tests

Both Rockwell-C hardness and Vickers micro-hardness measurements were performed on all specimens, except some specimens in alloy Type II where they were too soft for R-C measurement. The use of micro-hardness was to ensure there was no transformation of the metastable austenite to martensite by indentation.

Tensile tests were carried out on an Instron machine with a cross-head speed of 0.05 cm/min. Percent elongation to fracture was measured from a preset gage with marks 2 cm. apart.

D. Ms Temperature Measurement

The martensitic transformation temperature was measured by differential thermal analysis, where the apparatus used was very similar to that of Goldman,[16] et al.

E. X-Ray Quantative Measurement

There has been considerable work done using x-ray techniques to identify and measure the relative amounts of austenite in hardened steels.[17,18]

The basic principle involved is that the relative integrated intensity of each phase is proportional to the relative amount or volume fraction of that particular phase.

Zr filtered Mo tube was used in this study for a shorter scanning angle range, say, from 30° to 40°, and three well-separated peaks corresponding to $(220)_\gamma$, $(211)^\alpha$ and $(311)\gamma$ were obtained (because Mo radiation has short wavelength). The use of the austenitic peaks as proposed by Dietche was intended to average out the effect of preferred orientation that may exist in austenite, which could lead to serious errors in quantitative x-ray analysis.

For each peak, the diffracted intensity I is related to the volume fraction of that phase by:[19]

$$I = K\left(\frac{1}{v^2}\right) F^2 P L e^{-2m} V\left(\frac{1}{2\mu}\right) \quad \text{- - - - - - - - - - - - - - - (1)}$$

where K is a constant for a given experimental condition

v is volume of unit cell

F is the structure factor

P is multiplicity factor

L is the Lorentz-polarization factor

e^{-2m} is the temperature factor

V is volume fraction of the phase considered

$\frac{1}{2\mu}$ is the absorption factor for flat specimens

setting $R = \left(\frac{1}{v^2}\right) F^2 P L e^{-2m}$

then for the two-phase mixture,

$$I\gamma = R\gamma V\gamma \quad \text{- - - - - - - - -} \qquad (2)$$

$$I\alpha = R\alpha V\alpha \quad \text{- - - - - - - - - -} \qquad (3)$$

in addition

$$V\gamma + V\alpha = 1 \quad - \quad - \quad - \quad - \quad - \quad - \quad - \qquad (4)$$

combine (2) (3) and (4), and we have

$$V\alpha = \frac{(R\alpha/R\gamma)}{(I\alpha + (R\alpha/R\gamma)I\gamma} \quad - \quad - \quad - \quad - \quad - \qquad (5)$$

Thus, after putting suitable values for calculating "R" of $(220)\gamma$ $(311)\gamma$ and $(211)\alpha$ planes, the ratio of $R\alpha/R\gamma)$ can be obtained for both types of alloys in this work. It was found that for Type I alloy this ratio was ~ 1.35 whereas for Type II alloy, a value of ~ 1.42 was obtained.

The method for measuring relative integrated intensities was facilitated by the use of an automatic counting-rate printer which recorded at intervals the intensity of the radiation diffracted, thus the profile of the intensity peak was actually step-scanned and after substracting the background intensity, the integrated intensity could be readily estimated.

Some of the specimens were examined using a Norelco x-ray diffractometer with (200) -LiF crystal monochromator. This monochromatization device eliminated most of the x-ray fluorescence background, so that a CuKα target tube could be used.

F. Optical Microscopy

The specimens were electropolished in a 90% acetic and 10% perchloric acid first and subsequently etched in ferric chloride solution. The use of electropolishing rather than conventional mechanical grinding was to avoid possible phase transformation due to grinding the austenitic specimens. Electropolishing is also much faster.

Observation and photography were performed with a Carl Zeiss Optical

microscope.

G. Transmission Electron Microscopy

Thin foils for tranmission electron microscopy were prepared by first chemical thinning in a 1:1 H_2O_2 bath at ~ 5°C. Rapid initial electropolishing and good surface finish were obtained by using an electrolytic solution of 9 parts glacial acetic acid and 1 part perchloric acid, operating at 20 vdc at room temperature. Final thinning was performed by electropolishing in the well-known chromic oxide-acetic acid solution (135 ml glacial acetic acid, 25g chromic acid, 7 ml water) at 10 vdc and ~ 5°C.

A siemens Elmiskop IA microscope operating at 100 kV was used to observe the microstructures. Usually, a series of dark field image pictures of the same area were taken in order to avoid any ambiguities in the identificaiton of the phases present and in the interpretation of diffraction patterns.[20]

H. Scanning Electron Microscope

The use of scanning electron microscopy to observe the topography of fractured surfaces has only recently been widely applied. This technique possesses advantageous features over the conventional replica fractography in that: (1) Essentially no sample preparation is required and direct examination on the surface is possible. (2) Image formation is due to secondary electrons emitted from surface layer of ~ 100Å depth, so that a three-dimensional picture is obtained which facilitates image interpretation.

In this study, some fractured (in tension) surfaces were examined in a FELO U3 scanning electron microscope operating at 25 kV. The source of image formation was secondary electrons.

III. RESULTS

A. Martensitic Transformation Temperatures

(1) Type I alloy:

The Ms temperature of the as-deformed austenite was found to be about -85°C. However, after the annealing treatments of the metastable austenite, Ms temperatures as seen in Fig. 1 were raised due to carbide precipitation in austenite during the aging (depletion of Mo and C from matrix). This was confirmed by transmission electron microscopy as will be shown in a later section. In addition, from the variation in Ms temperature with annealing time a study of precipitation kinetics was possible, i.e., the annealing times required to achieve for a given Ms temperature at different annealing temperatures were calculated. It was found that the activation energy for this precipitation process was ~ 60 k cal/mole, which is of the right order of magnitude for diffusion of substitutional solute atom in γ iron, and is also very close to the value reported by Thomas, et al.[1] from Portevin-Le Chatelier effect.

(2) Type II Alloy:

As in the case of Type I, Ms temperatures were generally raised as a result of precipitation. However, after 500°C/1 hour aging, the Ms temperature was found to be lowered from ~ 60°C (the unaged austenite) to ~ 90°C, and consequently, the amount of martensitic phase transformed was smaller as detected by x-ray diffraction analysis (fig. 3). A possible explanation for the decrease in Ms temperature will be given in a later section.

B. X-Ray Diffraction Analysis

(1) Type I Alloy:

Fig. 2 and fig. 3 show respectively the x-ray diffraction profiles from the annealed austenite and transformed (by LN cooling) martensitic specimens. In fig. 2 the appearance of a martensitic phase can be seen as a result of annealing because Ms temperature was raised above room temperature. As a matter of fact, after 600°C/500 hour annealing, the specimens were rendered essentially martensitic. LN cooling the annealed austenite, it was found that although shorter annealing time, say, 600°C/7 hours, Ms temperature was raised appreciably, (fig. 1), the amount of retained austenite did not decrease (fig. 3) as would be expected. A plausible explanation for this will be given together with the results of the microstructural investigation and mechanical properties. In addition to the above observations, it is noted that there is a shift in peak position of the martensitic phase in fig. 2, i.e., an increase of ~ 0.2° in (2θ) valve for the lower two profiles. This increment in (2θ) value would correspond to a decrease in "d" spacing of the martensite lattice as required by the Bragg's law. This is thought to be due to the removal of solute atoms from the solution to form carbides on annealing, because the radius of Mo atom is larger than that of Fe atom. (1.36Å vs. 1.26Å).

(2) Type II Alloy:

Fig. 4 gives the volume fraction of martensite with different thermal treatments. Curve "a" shows the amount of martensite increasing almost linearly with time during annealing the austenite after a certain "incubation" period -- beyond which the Ms temperatures were above room temperature. Curves "b" and "c" both show an initial decrease and then a small but steady increase in the amount of martensite. As mentioned

earlier, there was a lowering in Ms temperature at this particular annealing stage which can accordingly account for the lowered α amount.

C. Mechanical Properties

(1) Type I Alloy:

The results of hardness measurements are shown in fig. 5(a). The dotted lines in the plot represent a two-phase mixture so that an abrupt change in hardness is observed. Fig. 5(b) gives the results of 0.2% flow stress of the martensite and in the case of austenitic condition, the upper yield stress. It is seen that there was a drop in yield stress upon annealing the deformed austenite. However, for the LN quenched martensitic specimens, the variations in flow stress are characteristic of the precipitation-hardenable alloys. This is a very interesting point and will be treated in a later discussion. Tensile strength values (UTS) are also plotted vs. annealing time in fig. 5(c). It appears that the strength levels increase on annealing the deformed austenite. This is due to the formation of strain-induced martensite as confirmed by its microstructure. Elongation curves for 2 cm gauge length of the specimens are given in fig. 5(d). It is seen that the as-deformed austenite has a very high elongation (55%) and, as the annealing progressed, the elongation values drop rather drastically, whereas the elongation values for the LN cooled specimens do not behave similarly to their "parent" phase, i.e., the curves are rather flat initially and decline very slowly at longer annealing time.

There are some other interesting features regarding the tensile properties. Firstly, there was a pronounced yield drop on the stress-strain curves for the as-deformed austenitic specimens, and this yield drop decreased in magnitude upon annealing at temperatures where the mechanical

properties showed significant changes, e.g. 600°C. Secondly, after several percent of straining the austenitic specimens, serrations appeared on the stress-strain curves, and audible click sound could be heard. This phenomenon is neither due to the Portelin-Le Chatelier effect as the testing temperature was too low (room temperature) to account for it, nor due to twinning as the product phase was ferromagnetic. Therefore, the serrations must be the result of formation of martensite during straining. Thirdly, for the austenitic specimens, if we consider the difference in strength values of the UTS and yield stress as an indication of the amount of work hardening contribution during the tensile test, then from fig. 6 we see that there is a linear increase in the amount of work hardening ($\Delta\sigma_{WH}$) with annealing time. The abrupt change in $\Delta\sigma_{WH}$ signifies the occurrence of a two-phase mixture. Fourthly, the difference in flow stress values of martensitic specimens with those of the corresponding austenitic specimens may be taken as an indication of the contribution due to martensitic transformation, i.e., $\Delta\sigma_{MT}$. Again, it appears that $\Delta\sigma_{MT}$ is linearly increased with the annealing time (fig. 7), which implies precipitation on annealing may enhance the strengthening effect of martensitic transformation.

(2) Type II Alloy:

Microhardness values and tensile properties of this alloy in austenitic and martensitic conditions at different thermal treatments are shown in fig. 8 (a), (b), (c) and (d). Dotted lines in fig. 8(b) represent the behavior of a mixed phase structure. It is evident that only 500°C annealing gives significant changes in mechanical properties, and for this reason, a detailed study of this alloy was done particularly at this temperature. Fig. 9(a) gives the variations in tensile properties with different isothermal

annealing time. It seems clear that changes in tensile properties were drastic in the early stage of annealing and leveled off at longer annealing time. This would imply that there is also a significant change in the corresponding microstructures as will be demonstrated in a later section. Fig. 9(b) shows the strengthening effect by tensile deformation, $\Delta\sigma_{WH}$ (due to strain induced martensite) and by LN cooling, $\Delta\sigma_{MT}$ (due to martensitic transformation) as a function of annealing time. It is noted that there is a definite increase of $\Delta\sigma$ values in both cases.

A comparison between the tensile behavior of this alloy with that of type I was also very interesting. Firstly, there was no yield drop at the onset of plastic deformation, and the deviation from linearity on the stress-strain curve occurred at much lower stress than that of Alloy type I (fig. 10). Secondly, there was essentially no or undetectable serration on the stress-strain curves in the work hardening region (fig. 10). Thirdly, a higher work hardening rate was exhibited for this alloy as compared with that of type I alloy [fig. 10 curves (1) and (3); (2) and (4)].

Finally, it is noted that the stress-strain curves of the as-annealed two-phase-mixture specimens were very similar to those of the LN cooled specimens, except in the case of type I alloy, where serrations appeared on the stress-strain curves just before necking occurred.

D. Optical Metallography

Fig. 11 (a), (b) shows the microstructures of the type I alloy in the LN cooled condition (a), and 600°C/7 hours annealed then LN cooled condition (b), respectively. It can be clearly seen that as a result of prior austenitic annealing, the average martensitic grain size was reduced

and the general darker etch of the structure upon subsequent cooling in LN, the later phenomenon was generally taken as an indication of precipitation of carbides in the alloy.

The morphology and distribution of strain induced martensite were also interesting: fig. 12(a) shows the morphology of strain-induced-martensite in regions above the gauge length, i.e. the portion in the specimen that is subjected to little deformation. It is seen that most of the martensite crystals have the form of "M" shape, whereas fig. 12(b) shows the martensite in the gauge length region that had been induced by straining up to 16% tensile deformation. It is observed that some of the martensite phase was apparently nucleated on or confined to the former austenite grain boundaries and their morphologies were more or less in the form of bundles of needle-shaped martensite crystals.

E. Transmission Electron Microscopy

(1) Type I alloy:

a. Microstructure of Austenite:

Fig. 13(a) shows the microstructure of the deformed (30% rolled at 500°C) austenite, it is obvious that there exists a high dislocation density, and this kind of distribution, i.e., tangled dislocations, would indicate that considerable cross slip had occurred as a result of deformation. Careful gun tilt dark field illumination could not reveal the expected precipitates uniquely, rather, only dislocations were in contrast. The diffraction pattern also did not show the precipitate spots. This is reasonable due to the small size of the precipitates and the possibility of nucleating them on the dislocations. In some regions, deformation twins were observed as confirmed by dark field selected area diffraction studies.

The twins were found lying on {111} planes.

Fig. 13(c) gives the structure of the austenitic alloy after annealing 7 hours at 600°C. The foil orientation was the same as in Fig. 13(a), i.e., [112]. It is seen that the dislocations have a tendency to arrange themselves into elongated cells of varied size approximately parallel to <110>, and the dislocation density in the cell walls is very high. Dark field on matrix spot (220) revealed the presence of very fine precipitates (~ 80Å), again the dislocations were also in contrast. A positive identification of the precipitates is not possible due to the small size and volume fraction of the precipitates. Annealing for a longer period rendered the structure partially martensitic, and thus will be shown in later sections. Annealing at 500°C showed a similar change in microstructure, although the kinetics were much slower.

b. Microstructure of Martensite:

Fig. 14(a), (b) shows typical microstructural features of the martensite phase obtained by LN cooling of the unannealed austenite, that is, the conventional ausformed martensite. In fig. 14(a), bendind or distortion of a martensite plate, presumably due to the interaction of the propagating martensite crystal during phase transformation with the pre-existing precipitate-decorated slip band in austenite, can be seen at "A," sharp ended martensite crystals at "B" and fine transformation twins at "C." In some cases, as seen in fig. 14(b), the twinned area seems to be at the mid-rib at "D" of the large martensite plate, whereas in the edge portion of the martensite plate, say at "E," a high density of dislocations was present. This would mean that two modes of lattice invariant shear co-exist in the same martensite plate. Work done on the deformation mechanism of

bcc crystals, or more specifically, ferrite crystals, has found that twinning is the favorable deformation mode at high strain rates and/or low temperatures. Since martensitic transformation could be considered as a special kind of plastic deformation, the first-formed martensite crystals, i.e., the central or mid-rib portions, were formed at high speed (high strain rate) and low temperature (low Ms temperature). It is obvious that twinning is a favorable mode for lattice invariant shear. The outer portions of the plate were formed later at slower speed and higher temperatures (because heat is generated as martensite crystals form), and consequently slip mode takes place. The microstructure of martensite formed by LN cooling of the 600°C/7 hours annealed austenite is shown in fig. 15 and fig. 16. Generally, a finer martensite grain size was observed which was also shown in optical microscopy (fig. 11), and the martensitic crystals seem to arrange themselves, or self-accommodate, in approximately the same orientation (fig. 15b). Frequently, dark field illumination usually revealed the presence of fragments of martensite crystals, e.g. at "F" in fig. 15(b), (c). Fig. 16 shows another area of the same specimen in [100] orientation, a magnified dark field picture on the {002} matrix spot, e.g. (b), (c) reveals uniquely the presence of fine precipitates, (~ 80Å). It should be mentioned here that the dislocation density in this case is still very high (fig. 15a, fig. 16a), although a quantitative measurement is impractical.

It is interesting to examine the martensitic structure when the parent austenitic phse contains sizable precipitates, say 200 ~ 300Å. However, with this size of precipitates or at longer annealing time at 600°C, e.g., 42-1/2 hours, the austenitic alloy transforms to martensite on cooling

to room temperature as mentioned in an earlier part of the thesis, and hence it was not possible to retain enough austenite to reveal its precipitation hardened structure. Fig. 17 shows that the presence of precipitates caused the martensitic boundaries to be irregular and less well-defined. In some cases, as shown at F in fig. 18, only fragments of the martensite plate are in contrast, indicating a change in orientation of the otherwise nearly flat plate, because tilting of the foil would observe the "continuing" view of the same martensite crystal. In addition to the above observations, up to this stage of annealing the precipitates were large enough to give rise to discernible diffracted spots and thus could be identified. Table II lists the results of the "d" spacings from several diffraction patterns. Within the limit of electron diffraction, the precipitates are identified as β-Mo_2C, a hexagonal close-packed phase. These precipitates are arranged in Widmanstatten patterns as shown clearly in dark field. (fig. 19c, d). Also, the morphology of the precipitates appears to be needle- or rod-like, as seen from the micrograph. The orientation relationship between the matrix, in this case, martensite, and Mo_2C rods is very interesting. The crystallographic features of hexagonal phase, e.g. β-Mo_2C and ε-carbides in bcc matrix are well documented.[21] Two different orientation relationships (differ by a rotation of 5° in the basal plane of the h.c.p phase) have been established thus far. The one given by Pitsch-Schrader[22] showed that:

$$(011)_\alpha \;//\; (0001)Mo_2C$$

$$(100)_\alpha \;//\; (2\bar{1}\bar{1}0)Mo_2C$$

$$[100]_\alpha \;//\;]2\bar{1}\bar{1}0]Mo_2C$$

with the $[100]_\alpha$ being the growth direction of the Mo_2C carbides. Since the misfit between the two phases is smallest (4.7%)[21] the other relationship was due to Jack[23] on ε-carbide in tempered martensite:

$$(011)_\alpha \;//\; (0001)_\varepsilon$$
$$(101)_\alpha \;//\; (1\bar{1}01)_\varepsilon$$
$$[1\bar{1}1]_\alpha \;//\; [1\bar{2}10]_\varepsilon$$

This was identical to the case of hcp Ni_3Ti precipitation with martensite in maraging steels.[24] For the present alloy, fig. 20 reveals that the orientation relationship by Jack is obeyed. This is not surprising because the precipitates must have formed already in austenite during annealing. (Ms temperature estimated by extrapolating in fig. 1 is found to be $\sim 50°C$ up to this stage of annealing). Upon transforming to martensite, the precipitates were not likely to be sheared because of their large size, and thus the observed orientation relationship should reflect a relationship between the precipitates and the matrix before phase transformation, i.e., austenitic phase. Because of the close lattice match between fcc austenite and hcp precipitates, it is expected that:

$$(111)_\gamma \;//\; (0001)\text{hcp}$$
$$[1\bar{1}0]_\gamma \;//\; [1\bar{2}10]\text{hcp}$$

whereas if the austenite transforms to martensite obeying the K-S relationship, namely,

$$(111)_\alpha \;//\; (011)_\alpha$$
$$[1\bar{1}0]_\alpha \;//\; [1\bar{1}1]_\alpha$$

as orientation relationship identical to the present result can be obtained. Similar results were also obtained in isothermal decomposition of Mo austenitic alloy recently.[25]

Specimens holding at still longer periods, e.g. 600°C/600 hours, the morphology of the precipitates change from rod to spheroids or rectangles. (~ 1000 ~ 2000Å), as seen in fig. 21. No orientation relationship

between precipitates and matrix could be found. The precipitates were identified by selected area electron diffraction as Fe_2MoC, an orthorhombic phase. Previous work on overaging reactions of Mo containing ferritic alloy steels[26] has shown that if the Mo/C ratio is more than about 20, the intermediate carbides $M_{23}C_6$ and M_aC_b form after Mo_2C and before M_6C and MoC. In the present case, the Mo/C ratio is about 17 and hence we see that the above rule might be applied to the austenitic phase as well.

(2) Type II alloy:

a. Microstructure of Austenite:

Quantitative x-ray (fig. 4), hardness and flow stress measurements (fig. 8) have indicated that the solution-treated specimens were austenitic. However, the transmission electron micrography and electron diffraction study showed that the thin foil was martensitic. This phenomenon was also observed by Garwood and Jones[27] in their work on 25% Ni, Ti, Al maraging steel, and was considered to be due to spontaneous transformation to martensite arising from stress relaxation at the foil surfaces during thinning.

Austenitic specimens annealed 500°C for one hour showed a structure which was mostly austenite. This means that the austenite was rendered more stable by the above annealing treatment and this may be confirmed from the fact that Ms temperature of the alloy at this stage of annealing treatment was lowered. Fig. 22 shows typical microstructures and its corresponding diffraction pattern. Both bright field and dark field illumination revealed the presence of very fine spherical particles. Precipitation in this system, viz. Fe-Ni-Ti and age-hardenable stainless

steel has been studied quite extensively due to their prominent high temperature mechanical properties.[11,28,29] It was shown that hardening in these alloys was attributed to the precipitation of metastable γ' particles, which are coherent with the matrix of composition and posses the $Cu_3Au(L1_2)$ ordered crystal structure. Coherency strain contrast in this case, however, could not be detected probably because the strain is very small, if any. Besides, many diffraction beams were operating which may also preclude the observation of strain contrast. This is in contrast to the similar age hardening Ni-Ti superalloys, where the lattice misfit between the γ' and matrix is large enough to reveal the coherency strain contrast, and the shape of the particles is cuboidal.[30] Some areas in the micrograph e.g. fig. 22(a) (b), show that the particles had a tendency to line up in approximately $<110>_\gamma$ direction, probably indicating the initial formation stage of the more stable hexagonal Ni_3Ti Widmanstatten phase. This presumption is not unreasonable, since faulting in α' particles could lead to the in-situ formation of the hexagonal phase in the same way as it might happen in certain maraging alloys.[20]

After 3 hours annealing at 500°C, the structure was partially martensitic and hence will be treated in the next section.

b. Microstructure of Martensite:

For the sake of clarity, this section will be divided into two groups, namely, (i) transformation of martensite by ausaging only, (ii) further transformation by LN cooling.

(i) Transformation by ausaging:

Fig. 23 shows the structure after 500°C/3 hours annealing treatment; the bright field image (a) clearly reveals the spherical particles, martensite plate "M" and line-up particles at "A;" the selected area

diffraction pattern (c) indicates a K-S relationship and superlattice diffraction spots at circled area. However, another area of the same foil shows that the orientation relationship between the matrix$^{(bcc)}$ and the fcc precipitates is N-W, namely $(110)_m \,/\!/\, (100)_p$, $[1\bar{1}2] \,/\!/\, [011]p$, as seen in fig. 24(c). No apparent reason could be given for this observation. The possible speculations are (1) uncertainties of orientation determination by electron microscopy, since the K-S and N-W relationships differ only by 5° 16', (2) either of the K-S or N-W related martensite crystals is in the transition state, i.e., subjected to different "environment" which makes the rotation of 5° 16' possible as in the case of martensite nucleation in 304 stainless steel.[34] In some regions of the foil, discontinuous or cellular precipitation could be seen adjacent to the grain boundaries, e.g., fig. 25. The orientation relationship between the martensite matrix and the lamellae precipitates, identified by electron diffraction as hcp Ni_3Ti, is:

$$(0001)Ni_3Ti \,/\!/\, (011)_\alpha$$

$$[1\bar{2}10]Ni_3Ti \,/\!/\, [1\bar{1}1]_\alpha$$

i.e., the Jack relationship, which also reflects the original relationship of the hcp precipitate with the fcc austenitic matrix lattices being closest matching. Fig. 25(b) also shows streakings on the Ni_3Ti spots, the direction of the streaks is parallel to [0001] Ni_3Ti and of course, perpendicular to the lamellae precipitates. This type of boundary precipitation is generally known to be very detrimental to the ductility of the material as evidenced by the low elongation value at this stage. Longer time annealing at 500°C causes the growth of the spherical particles, cellular precipitates, and the zig-zagged martensite crystals.

(ii) Transformation by LN cooling:

The micrograph of LN cooled unannealed austenite shows typical substructure of the low-carbon, or dislocated lath martensite (fig. 26), where most of the martensite crystals are arranged in bundles within which they misorient slightly.

Fig. 27 provides the micrographs of 500°C/1 hour annealed, LN quenched structures. It is seen that the grain is distorted and size finer than that in fig. 26, presumably due to the presence of fine precipitates as shown clearly in dark field (c), (d). Fine scale twins lie perpendicular to $\langle 112 \rangle_\alpha$ are also seen in both bright and dark field pictures. Fig. 28 shows a magnified view of a martensite crystal, plastic deformation of its surrounding matrix by the martensite plate is easily seen and according to Christian[32] this will lead to stabilization of the martensite plate by losing some coherency of the glissile interface.

The microstructures of the 500°C/3 hour annealing LN quenched-specimen are in general almost indistinguishable from fig. 23, 24, and hence will not be shown here.

c. The growth of γ' precipitates:

The kinetics of growth of γ' particles in Ni-base superalloys has been studied in detail over the past decade and recently by Ardell.[30] It is generally recognized now that the growth of γ' particles is by diffusion-controlled coarsening. Fig. 29 shows a plot of particle radius vs. (annealing time)$^{1/3}$; although we have only three data points it is seen that a straight line is obtained in accordance with the Lifshitz-Wagner equation,[33] namely,

$$r^3 - r_o^3 = \frac{8D\gamma Co^2}{9RT} \quad t \quad \text{where}$$

Co = the equilibrium solubility of large precipitates

= volume of precipitate per mole of solute

γ = interfacial energy of the solute-matrix interface

Ro = intitial radius of the precipitates

(3) Microstructure of Strain-Induced Martensite in Type I Alloy:

Fig. 30(a) shows the morphology of strain-induced martensite in the region above gauge length of the tensile specimen, this is consistent with the light micorscopic examination where "M" shaped martensite was frequently observed (fig. 12a). Similar "M" shaped morphology was also seen in the alloy after 16% tensile elongation as shown in fig. 30(b). Fig. 31 demonstrates the K-S orientation relationship between the austenitic matrix and strain induced martensite. It is noted that in fig. 31(d) the martensite crystals were dispersed in the matrix. Fig. 32 shows the neddle-like martensite morphology, which also was observed by light microscopy (fig. 12b). These martensite needles are arranged parallel in groups of two directions, the areas between two adjacent needles are austenitic matrix containing high dislocation density.

Of all the strain induced martensite crystals observed thus far, in no case was any internal twinning found, even though the LN quenched martensite of the same alloy showed some twinning (fig. 14).

F. Scanning Electron Microscopy

The modes of failure in metals can be roughly characterized by the names cleavage, dimple rupture (or microvoid coalescence), fatigue and intergranular separation. Usually, combinations of the fracture modes are also observed.

Fig. 33(a), (b), (c) and (d) show the fractographs of tensile broken

surfaces of Type I alloy, annealed at 600°C/7 hours as annealed (a), (b) and LN cooled (c), (d) respectively. It is to be noted that strain induced martensite occurs in (a) whereas in (c), the martensite is formed by LN cooling. Both types of martensite structure show a dimple fracture mode, or microvoid coalescence. However, fig. 33(a) indicates the degree of necking around the dimples is generally higher than that in (c), although the dimple size is similar in both cases.

For type II alloy, the fractograph of unannealed sample is shown in fig. 34. It is seen that a dimple mode fracture developed with a size much larger than the type I alloy. After 500°C/1 hour annealing, the fracture mode shows a mixture of dimple, quasi-cleavage and intergranular, as seen in fig. 35. In addition, the necking of the dimples in fig. 35(c) is decreased as compared with fig. 34(a). Fig. 36 shows the fractured surface of the LN cooled unannealed sample, where the dimples are also shallower than those in fig. 34(a). LN cooled, 500°C/1 hour annealed sample again shows a mixed mode of failure, i.e., shallow dimples and flat grain boundary fracture path (fig. 37).

IV. DISCUSSION

A. Recovery and/or Recrystallization of the Ausformed Austenite

It has been well established that the presence of dispersed second phases can either accelerate or retard the softening of the deformed structure on annealing.[34] Recent work[35] has shown the inter-particle spacing is the determining factor of this effect regardless of the particle size or volume fraction of the precipitate. Large interparticle spacing caused an acceleration effect whereas considerable retardation was encountered when the spacing was reduced.

In the present study, upon annealing the high dislocation density austenite, two simultaneous events are believed to occur: (1) the growth of the precipitates, which can be promoted by pipe diffusion via dislocations, (2) disentangling of the dislocations from particles, rearrangement of dislocations into low energy configurations and/or short range annihilation of the dislocations. There is a close relationship between the above two events as the precipitates form and grow, namely, (1) the stacking fault energy of the matrix is raised due to solute atom depletion, which will assist cross-slip climb and hence rearrangement of the dislocations, (2) reduced surface free energy by coalescence of smaller precipitates can also provide driving force for the redistribution of dislocations. The net result of the annealing was that elongated dislocation cell structure developed where the cell wall consisted of high dislocation tangles contained in {111} planes (fig. 13c).

Recrystallization, defined as the sweeping of high-angle boundaries through the deformed crystal in order to create strain-free regions behind the moving front, did not seem to occur to any detectable degree in this case. The possible reasons are: (1) pinning and thus immobilization of the subgrain boundaries by precipitates, (2) competitive nature of the recovery and recrystallization behaviors described by Nobili et al.[36] in the study of the recrystallization of SAP alloys. (3) the uniform, homogeneous distribution of dislocations by ausforming in the structure causes less lattice misorientation and hence less nucleation sites for effective recrystallization.

The flow stress of the austenite did show a slight decrease as a result of annealing and may be attributed to the redistribution of dislocations in the microstructure. Detailed analysis is complex

because two opposing mechanisms are operating, namely, precipitation hardening and the larger "cell" size. The latter was shown to follow $\nabla = kt^{-1/2}$ (t: cell diameter, k = constant),[37] where the dislocation pile-ups were thought to determine the strength of cell substructures.

B. Effect of Austenite Structures on the Subsequently Transformed Martensite -- Kinetical:

It is generally accepted that the defect structure of the austenite, e.g. dislocation density, controls the kinetics of subsequent martensitic transformation.[38] For instance, the number and size of martensitic embryos, the propagation of the embryos, etc. are closely dependent on the austenitic condition. A high dislocation density is associated with a low Ms temperature and a high initial rate of martensite formation.[39]

However, little attention has been received as to the effect of precipitates or dispersoids on the martensitic transformation, both kinetically and especially, structurally. Before going to the specific details, general features of the effects of pre-existing precipitate on martensitic transformation will be discussed:

(1) Nucleation of martensite:

The presence of precipitate in the metastable austenite usually will tend to promote the formation of martensite by providing suitable nucleating sites, because (a) chemically, regions in the vicinity of precipitates are known to be solute-atom depleted and hence are energetically more stable with respect to martensitic phase, i.e. they are potential areas for the formation of martensite once the driving force for transformation is large enough. (b) mechanically, precipitates

will either elastically strain the surrounding austenitic matrix (which is valid for coherent, partially coherent and incoherent) or cause plastic flow in the matrix near the precipitates. Since martensite embryos are usually considered as strain embryos, these strain centers in the austenitic matrix are thought to be regions where the restraining force for martensite formation is minimum and naturally, whenever the chemical driving force is large enough, martensite phase will form in these regions. From the arguments of both (a) and (b), we may expect a more or less controlled and uniform distribution of martensite phase by transforming a dispersion hardened austenitic phase.

(2) Growth or propagation of martensite:

Because of the compatibility and continuity between lattices of the martensite phase and austenitic matrix, the latter must be plastically deformed by the growing martensite crystals. Since a dispersion hardened austenite has a higher flow stress than the single-phase austenite, we may expect that the growth of martensite crystals in the strengthened austenitic matrix must be impeded to some extent. The result is that the martensite crystal size tends to be smaller and the arrangement of martensite crystals may be in such a way that they grow only on certain crystallographic habit planes and/or self-accommodated in bundle forms in order to minimize the resultant strain energy of the system.

Hornbogen and Meyer[40] found a decrease in Ms temperature of a γ' precipitated austenite after short aging times at 600°C and they attributed this effect to the shearing of the f.c.c. precipitate to a b.c.c. structure when the austenite was transformed to martensite. Presumably excess energy was required to shear these particles to a new crystal structure. A similar effect i.e., lowering in Ms temperature, was also obtained in

the present study, so that it is very interesting to examine how a fine coherent precipitate in austenite can change the value of free energy change when the austenite-martensite transformation occurs.

Let us consider a homogeneous austenitic solid solution with a Ms temperature and total driving force or free energy change ΔG_s for martensitic transformation, Ms and To [the equilibrium temperature at which free energies of austenite and martensite are equal, approximately taken as 1/2 (As + Ms)] are usually known to increase with decreasing amounts of solute whereas the measurement of ΔG_s is generally taken as the magnitude of (To-Ms), and hence decreases moderately with decreasing solute concentration. With this fact in mind, we now consider the annealing or aging effect of the alloy. As soon as precipitation occurs, because of the solute atom depletion from the matrix, the Ms temperature is raised and ΔG_s reduced in the manner described above. But in addition to this change in properties of the matrix, the effect of precipitate per se must be considered. Two possibilities may occur when the austenite containing fine coherent f.c.c. precipitates transforms to martensite: (1) the precipitates are deformed or sheared in conforming with the surrounding austenitic matrix. (2) the precipitates are not sheared during martensitic transformation of the austenite. These two alternatives are shown schematically in fig. 38, where the martensitic transformation is simulated by a simple homogeneous shear. The possibility (1) would involve the energy consumed to allow for the shearing of the precipitates, whereas the possibility (2) would require the rearrangement for mass surrounding the particles which essentially creates a high energy incoherent interface between the matrix and particles. Thus, the final effect will be determined by the balance of these two

possibilities. To state in a more quantitative way, we take the radius of the precipitates as r, the number of precipitates per unit volume as N, the high energy interfacial energy per unit area of the interface as γ and the free energy needed to shear the precipitates per unit volume of the deformed precipitate as ΔG_v. Then the free energy change for possibility (1) is $\Delta G_1 = \frac{4}{3} \pi Nr^3(\Delta G_v)$ and for possibility (2), $\Delta G_2 = 4\pi Nr^2\gamma$. It is seen that for small values of r, ΔG_1 is smaller than ΔG_2 and accordingly, shearing of the precipitate is preferred because the total free energy change for the system $\Delta G_t = \Delta G_s + \Delta G_1$ would be more negative. The critical radius for the shearing of precipitates is then $r_c = 3r/\Delta G_v$ by simply equating ΔG_1 and ΔG_2.

From the above discussion, the lowering of Ms temperature in the present study could possibly be explained as the extra driving force needed to shear the precipitates. But as the precipitates grow coarser, or above r_c, where deformation of the precipitates does not occur, the raising of Ms temperature due to solute element depletion becomes predominating and overpowering the possible decreased Ms temperature on forming incoherent interface on transformation. The variation in Ms temperature by precipitation has been treated in the consideration of austenite stabilization in the past years, for example, the destruction of martensite embryos by precipitation,[41] locking of the martensite/austenite interface by solute atoms segregation,[42] the strengthening effect of the austenite matrix by strain-aging processes,[43] etc. But all the models for stabilization of austenite are concerned with the segregation of interstitial solute atoms, which is not the case in the present study. The whole argument mentioned so far could be looked upon from another point of view, as hinted by Shewmon.[33] The net free energy change ΔG for martensitic

transformation could be taken as analogous to the work done by stress applied to plastically deform the austenite, except the work hardened product is martensite. Then the presence of precipitates will serve to resist the plastic flow and hence the interparticle spacing d is an important parameter. Below a critical d_c value, plastic flow or transformation will not occur unless more stress or energy is added to the system. In the case of precipitation hardening by coherent particles, there exists a critical r_c radius (for a given volume fraction of precipitates) which denotes the change from a dislocation cutting mechanism to a by-pass mechanism.[44] The value of r_c is $2Gb^2/\pi E$ (by equating $\tau_c = \frac{\pi Er}{2bd}$ for cutting and $\tau = \frac{Gb}{d}$ for by-passing), where E is the energy per unit area of the planar fault generated after cutting, G is shear modulus and b is Burger vector. We see that r_c obtained in this way is essentially the same expression as deduced previously from free energy considerations, with Gb^2 (the line tension of dislocations) corresponds to the high energy interfacial energy γ after martensitic transformation and E corresponding to the free energy change due to shearing of the precipitates ΔG_v.

C. Effect of Austenite Structures on the Subsequently Transformed Martensite - Structural:

Defect substructures in the austenite are usually considered to be inherited in the subsequently formed martensite lattice and hence contribute partly to the strength of the ausformed martensite.[1] In addition to this, the decoration of solute atoms or fine precipitates on the defect structure of the austenite, such as dislocations, twins, stacking faults, cell walls, etc., constitutes a semi-permeable or impermeable

barrier to the growth of martensite plates. Thus, the martensite grain size tends to be finer and its shape is distorted.

Now, let us consider the effect of particles in the austenite on the structure of transformed martensite. If we consider the martensitic transformation as a special kind of plastic deformation, which is quite reasonable due to the work-hardened structure of the martensite, then this problem becomes very similar to the case of studying work-hardening behavior of dispersion-hardened crystal, except the latter does not involve a change in crystal structure. Lewis and Martin[45] showed that for a given strain, the decrease in interparticle spacing resulted in an increased dislocation density for internally oxidized Cu. Later, Ashby[46] presented a theory of work hardening in dispersion-hardened single crystals, where he attributed the source of work hardening to the generation of secondary dislocations around each dispersed particle during straining (provided the particles do not deform plastically), and the impediment of primary glide dislocations by these secondary forest accounted for the increment of applied stress above the yield stress. Recent work on electron microscopy of the effect of dispersed phases on dislocation distribution in plastically deformed copper single crystals by Humphreys and Martin[47] has shown that at stage I, dislocations cross-slip at the particles whereas at stage II a more homogeneous distribution of dislocation substructures developed by the presence of particles. For the case of martensitic transformation, a simplified schematic model in fig. 38 may help to illustrate the role of particles. Suppose we take the particle out and hence leave a spherical hole in the austenite matrix. Then upon martensite transformation, the spherical

hole will be deformed into a shape conforming to the matrix (in this model, an ellipsoid shape), however two situations could happen to the particle: (1) if the particle deforms in the same way (shape) as the matrix, then after putting the particle back in the hole of the "new" matrix, only elastic strains due to coherency and volume change of the matrices would probably exist. 2) if the particle does not deform, or is more rigid than the matrix, then on putting it back into the hole, rearrangement of the mass at the particle-matrix interface must occur, i.e., plastic deformation by the generation of dislocations and other kinds of defects. Of course, the above description is over-simplified, because martensitic transformation is not just a simple homogeneous shear, but a complex deformation of the austenite involving lattice invariant deformation and dilation. Nevertheless, general features of the particle effect could be realized.

In summary, if the particles do not deform with the matrix during martensite transformation, a higher defect density martensite structure could be obtained than that of ordinary transformed martensite. The higher density of defects, such as dislocations, etc. are thought to be generated at the particle-matrix interface, multiplied by cross-slipping at the particles and by prismatic punching. It is also possible that dislocations in the martensite are heavily jogged during phase transformation by the presence of particles.

D. Strain-Induced Martensite

From fig. 10, we see that the tensile behavior of austenite in type I and type II alloys are quite different, namely, (1) a higher work hardening rate for type II alloy and this tendency is enhanced by the presence of

second phase particles. (2) serrations on the type I alloy tensile curves. These phenomena could be explained on the basis of the stability of the austenite phase in both types of alloy as follows. When deformation is performed on the specimen, the austenite will usually be deformed by slip as normal f.c.c. metals do. But when deformation is done below Md temperature, martensite phase will tend to form during deformation once the applied stress level is high enough to trigger its transformation. Thus a competition between the tendency for the austenite to slip and transform to martensite occurs during straining, and whatever mode predominates will control the straining process. For type I alloy, because of the presence of high density of dislocation substructure and fine precipitates by ausforming, it is expected that both mechanical stabilization (restraining force on the formation and growth of martensite) and chemical stabilization (depletion of solute elements from matrix by precipitation) occurred, which render the austenite to be more stable and hence the formation of martensite is made more difficult. Upon straining, the austenite would deform by slip and then work-harden, until the internal stress built up was sufficient to induce the formation of martensite. After that, slip occurs again until another group of martensite crystals with higher energy of formation formed, this process would repeat itself up to the point of necking of this material. Because the tensile curves actually consist of slip deformation of the austenite and the intermittent formation of martensite, the latter is thought to be responsible for the serrations on the stress-strain curves. The stability of austenite in type II alloy is considerably lower than that of type I, as evidenced by the automatic transformation to martensite on thinning the specimen, so that the formation of

martensite is the easy mode of deformation and the smoothness of the tensile curves is the result of continuous formation of martensite upon straining. Also, the higher work hardening rate in this type of alloy could be explained by this effect.

As for the effects of precipitate particles on the tensile behavior or the formation of strain induced martensite, it is seen that the work hardening rates are increased in both types of alloy, although the total elongation is reduced. The particles serve to increase the dislocation density in austenite and enhance the formation rate of martensite in the way described in earlier sections which could account for the observed higher work hardening rates.

E. Mixed Phase of Martensite and Austenite

It has been shown by Mangonon and Thomas [15] that the yield strengths of 304 stainless steel are linearly proportional to the volume fraction of α irrespective of the treatment used to form α, i.e., either stress nucleated or by thermal aging. Furthermore, the strength of the above system was better described as a special kind of composite strengthening due to the fact that the hard martensite crystals were too large in size (and large interparticle spacing) to be accounted for by a dispersion hardening mechanism.

In the present case, after annealing the austenite to a certain extent, precipitation and the partial formation of martensite occurred simultaneously, and the whole system is actually composed of three phases. However, precipitation took place on a scale much finer than that of martensite (as seen in micrographs). The latter is not likely to effect

the movement of dislocations as compared to the fine precipitates during deformation, so that it is interesting to see the strengthening of both austenite and martensite on the overall behavior of the "composite." The data of type II alloy are replotted in fig. 39. It is seen that the "simple law of mixture" is still obeyed and the lines are displaced to high strength levels depending on what extent the austenite and martensite are strengthened.

F. Correlation of Structure and Mechanical Properties

(1) Type I alloy:

The flow stress of the as-ausformed austenite could be accounted for primarily by the large amount of dislocations introduced by ausforming. After LN cooling, the strength of ausformed martensite is also controlled by the high density of dislocations as discussed by Thomas et al.[1] However, as seen clearly in fig. 5(b) and fig. 7, the difference in flow stress values of the martensite and austenite as a function of annealing time increases, which may imply that although the strength of austenite is decreased by annealing (the effect of recovery overriding that of precipitation hardening), the corresponding strength of martensite is increased. The increasing in flow stress of martensite could not be attributed to the precipitation hardening, since the material is already in a work hardened state after martensitic transformation. Rather, the precipitates are functioning indirectly on increasing the dislocation density during phase transformation in the ways described earlier and, accordingly, the strength of martensite is actually controlled by the dislocation density per se. In fig. 5(d), we see that the ductility of

the martensite as measured by elongation does not decrease, although the strength is increased. This is thought to be the result of finer martensite grain size and a more homogeneous distribution of dislocation substructures by the presence of particles. In addition to the above reasons, a decrease in tetragonality of the martensite due to carbide precipitation may also play a role in increasing the ductility.

(2) Type II Alloy:

The flow stress of the unannealed austenite is typical of the intrinsic strength of fcc alloys with the combination of solid solution hardening, grain size and moderate dislocation density. The martensite structure transformed by LN cooling also shows a typical dislocated martensite structure as in low-carbon maraging steels[24] and the flow strength can be explained solely by the dislocation density present from martensitic transformation. On annealing (for example, 500°C/ 1 hour), the flow stress of austenite increases and the corresponding microstructure as in fig. 22 shows the precipitation of very fine particles (~ 80Å), with interparticle spacing of 150 ~ 250Å. Simple calculation by Orowan criterion shows the predicted strength with this interparticle spacing is much higher than that actually measured, so that it is possible that the cutting or shearing mechanism is operating. The latter assumption may be supported by the fact that the flow stress is of the order of the stress calculated for shearing, i.e. $s = \pi \frac{\gamma r}{db}$, where d is interparticle spacing, r is particle radius, γ is surface energy (approximately the same as antiphase boundary energy in this system, ~ 150-200 erg/cm^2). After martensitic transformation, however, the increase in flow stress of the martensite does not have

the same rate as that of the parent austenite, but shows an increased slope [fig. 9(a) and (b)]. This means that other strengthening effects may be operating aside from the intrinsic strength of martensite and dispersion hardening (assume to be the same as in austenite), which may include the increased dislocation density, coherency strain, etc.

(3) Strain Induced Martensite:

The excellent ductility combined with high strength of TRIP steels was thought to be due to the delaying of necking of the material by introducing barriers stronger than dislocation tangles -- martensite, during straining.[48] The precipitates tend to increase the extent of work hardening attainable by the formation of strain induced martensite. Hence it is suggested that if the precipitation process could take place dynamically during straining and at the same time induce the formation of martensite (the latter could be achieved by adjusting Md temperature), an alloy with good creep-resistance may prove to be useful.

Since deformation twinning has been observed in the as-ausformed austenite in this study, it is suspected that the observed needle-like morphology of the strain-induced martensite (fig. 32) might have some correlation with it, for example, the in-situ formation of martensite on the deformation twins in austenite, although no direct evidence has been found yet.

Fractographs of the ausformed austenite shows a large extent of necking around dimples, which may indicate the delaying of necking during microvoid coalescence and thus has higher ductility.

V. SUMMARY

(I) Type I Alloy:

Upon annealing the deformed austenite, the following events occur:

(1) Ms temperature of the specimens is raised. A kinetic study of this phenomenon shows an activation energy of $\sim$ 60 Kcal/mole, which indicates the raise in Ms temperature is associated with the precipitation process involving substitutional solute elements (in this case, Mo).

(2) Values of flow stress decrease gradually; the microstructure shows the presence of fine precipitates and the development of dislocation cell structures. The latter is presumably the result of recovery.

(3) Higher work hardening rate is exhibited on the serrated stress-strain curve probably due to the precipitation of carbides.

On transforming the annealed austenite to martensite:

(1) The flow stress of the martensite increases gradually with no appreciable decrease in ductility; this is explained by the increase in dislocation density by the presence of precipitates, the finer martensitic grain size and fragmentation of martensite crystals.

(2) The precipitates, identified as Mo_2C, arrange themselves in a Widmanstatten pattern and have a definite orientation relationship with the b.c.c. matrix: $(\bar{1}11)_\alpha \;//\; (0001)_{Mo_2C}$

$$(101)_\alpha \;//\; (1\bar{1}01)_{Mo_2C}$$

$$[1\bar{1}1]_\alpha \;//\; [1\bar{2}10]_{Mo_2C}$$

This relationship could be accounted for by the way the precipitates occur in the matrix austenite.

(3) The presence of precipitates causes the martensitic boundaries to be irregular and less defined.

A comparison of fractured surfaces of tensile broken austenitic

specimen (strain-induced martensite) and LN cooled martensitic specimen shows a deeper necking of the dimples exhibited in the former case, which reflects a higher ductility.

(II) Type II Alloy:

Ausaged State

(1) The flow stress of the specimens in the early aging period could be accounted for by the shearing of small fine coherent precipitates during deformation.

(2) The lowering of Ms temperature could be due to excess energy required to deform the precipitates.

(3) The precipitates grow by diffusion controlled coarsening in accordance with the Lifshitz-Wagner equation.

(4) There are no serrations on the stress-strain curve by the formation of martensite on straining.

Ausaged and Transformed State

(1) As in the case of Type I alloy, the microstructure of specimens transformed from dispersion-hardened austenite consists of distorted, fragmented martensite crystals and fine precipitates.

(2) Whether the precipitates deform with the matrix or not during martensitic transformation the strength of resulting martensite always increases although greater strengthening effect would be achieved for the non-deformable precipitates.

(3) Discontinuous or cellular precipitation takes place at longer aging time which probably is the cause of brittleness in tensile tested specimens. Fractographic studies show mixed mode of intergranular and transgranular fracture.

(4) The flow stress of mixed phases of martensite and austenite

shows a linear increase with the volume fraction of martensite phase, despite the fact that the strength levels are raised by the substructural strengthening of both phases.

VI. CONCLUSIONS

1. It is shown that although softening of the ausformed austenite occurs on annealing, the corresponding strength of the transformed martensite shows an increase. This is explained on the basis of increased dislocation density due to the presence of precipitates on annealing. Hence, the enhancement of substructure strengthening of martensite is made possible by pre-dispersion hardening the austenite.

2. It is suggested that the conventional ausforming process could possibly be modified by less deformation of the austenite to enhance the kinetics of precipitation, followed by proper annealing treatment to get optimum particle size and spacing for obtaining maximum dislocation density upon quenching to martensite.

3. The good ductility of the ausformed martensite could be explained by the homogeneous distribution of dislocation refined martensite grain size and the decreased tetragonality of martensite lattice.

4. The decrease in Ms temperature of the austenite containing fine coherent precipitates could be accounted for by the extra driving force needed to deform the precipitates.

5. Whether the precipitates deform with the matrix or not during martensitic transformation, there always exists a strengthening effect on the final product. However, greater effect is exhibited for the non-deformable precipitates.

6. The precipitates will not only strengthen the martensite substructurally, but also refine the grain size and/or cause their irregular interfaces.

7. The presence of particles causes a higher work hardening during the strain induced martensitic transformation.

8. Higher stability austenite exhibits serrated stress-strain curves whereas a smooth curve is shown for the low stability austenite. This is accounted for by how difficult the martensite can be nucleated.

9. The mixed phase structure could be described as a "composite," although the strength levels are raised by strengthening both austenite and martensite.

TABLE II

Interplanar Spacings of the Precipitates: from Alloy I

Thin Foil	Martensite	β-Mo_2C	
D(Å)	d(Å)	d(Å)	hk.ℓ
		4.724	00.1
2.6 (P)*		2.600	01.0
2.36 (P)		2.362	00.2
2.28 (P)		2.278	01.1
2.027	2.027	2.278	01.1
1.71 (P)		1.748	01.2
		1.575	00.3
1.49 (P)		1.501	11.0
1.43, 1.43 (P)	1.433	1.431	11.1
		1.374	01.3
1.31		1.300	02.0
1.27		1.267	11.2
1.25		1.253	02.1
1.17, 1.18 (P)	1.170	1.181	00.4
		1.139	02.2
1.08 (P)		1.087	11.3
	1.013	1.075	01.4
		1.003	02.3
0.97 (P)	0.906	0.983	12.0

* (P) means precipitate

ACKNOWLEDGEMENTS

The author is deeply grateful to Professor Gareth Thomas for his guidance, encouragement and support during the research. He is also indebted to Professor E. R. Parker and Dr. P. R. Okamoto for helpful discussions. Thanks are also due to Mrs. Carol Zum Brunnen for her efforts and patience in typing the manuscript.

This work was supported by the United States Atomic Energy Commission through the Inorganic Materials Research Division of the Lawrence Radiation Laboratory.

REFERENCES

1. G. Thomas, D. Schmatz and W. Gerberich, "High Strength Materials," John Wiley and Sons, New York, p. 284 (1965).
2. O. Johari and G. Thomas, ASM Trans. Quart., 58, 563 (1965).
3. L. Raymond and W. Reuter, Acta Met., 12, 948 (1964).
4. T. Araki, S. Watanabe and H. Miyaji, Proceedings of the International Conference on the Strength of Metals and Alloys, p. 111 (1967).
5. E. B. Kula and C. F. Hickey, AIME Trans. 230, 1707 (1964).
6. E. B. Kula and J. M. Dhosi, ASM Trans. 52, 321 (1960).
7. I. Tamura, Trans. ISIJ, Vol. 6, 249 (1966).
8. A. J. McEvily, R. H. Bush, F. W. Schaller and D. J. Schmatz, ASM Trans., 56, 753 (1963).
9. V. F. Zackay and W. M. Justusson, "High Strength Steels," special report 76, Iron and Steel Institute, p. 14 (1962).
10. R. Phillips and W. E. Duckworth, "High Strength Materials," John and Wiley, New York, p. 307 (1965).
11. P. K. Pitler and G. S. Ansell, ASM Trans. 57, 220 (1964).
12. V. F. Zackay, E. R. Parker, D. Fahr and R. Busch, ASM Trans. 252, 60 (1967).
13. V. F. Zackay and E. R. Parker, Sci. American, 219, 36 (1968).
14. K. W. Andrews, JISI, 721 (1965).
15. P. L. Mangonon, Jr. and G. Thomas, UCRL-18869 (In press) AIME Trans.).
16. A. J. Goldman, W. D. Robertson and D. A. Koss, AIME Trans. 230, 240 (1964).

17. R. L. Miller, ASM Trans. 57, 892 (1964).

18. H. R. Erard, "Advances in X-ray Analysis," Plenum Press, New York, p. 256 (1963).

19. B. D. Cullity, "Elements of X-ray Diffraction," Addison-Wesley, Mass. (1956).

20. G. Thomas, I-Lin Cheng and J. R. Mihalisin, ASM Trans. Vol. 62, 852, (1969).

21. D. J. Dyson, S. R. Keown, D. Raynor and J. A. Whiteman, Acta Met. 14, 867 (1966).

22. W. Pitsch and A. Schrader, ARch. Eisenhitt.Wes. 29, 715 (1958).

23. K. M. Jack JISI, 169, 26 (1951).

24. I-lin Cheng and G. Thomas, ASM Trans. 61, 14 (1968).

25. F. G. Berry, A. T. Davenport and R. W. K. Honeycombe, "The Mechanism of Phase Transformation in Crystalline Solids," Proceedings of the International Symposium, Monograph and Report Series No. 33, p. 288 (1969).

26. J. H. Woodhead and A. G. Quarrell, JISI, 605 (1965).

27. R. D. Garwood and R. D. Jones, JISI, 204, 512 (1966).

28. B. R. Clark and F. B. Pcikering, JISI, 70 (1967).

29. L. K. Singhal and J. W. Martin, Acta Met. 16, 967 (1968).

30. A. J. Ardell, Metallurgical Trans. 1, 525 (1970).

31. P. L. Mangonon, Jr. and G. Thomas UCRL-18868 (submitted to AIME Trans.).

32. J. W. Christian, JISI Special Report 93 (London) 1 (1965).

33. P. Shewmon, "Transformation in Metals," McGraw-Hill (1969).

34. R. W. Cahn, "Physical Metallurgy" Morth-Holland Publ. Co. 925 (1965).

35. F. J. Humphreys and J. W. Martin, Phil. Mag. 14, 775 (1966).

36. D. Nobili, F. Mezzetti and E. Susi De Maria, J. of Matl. Sci. 3, 282 (1968).

37. C. J. Ball, Phil. Mag. 7, 1011 (1957).

38. J. W. Christian, "The Mechanism of Phase Transformation in Crystalline Solids," Proceedings of the International Symposium Monograph and Report Series No. 33, 129 (1969).

39. A. S. Sastri and D. R. F. West, JISI, 138 (1965).

40. E. Hornbogen and W. Meyer, Acta Met. 15, 584 (1967).

41. K. A. Malyshev and M. M. Vasilevskaya, Physics and Metals Metallography, 18, 150 (1965).

42. J. Woodilla, P. G. Winchell and M. Cohen, AIME Trans. 215, 849 (1959).

43. E. R. Morgan and T. Ko, Acta. Met. 1, 36 (1953).

44. G. Luetjering and S. Weissmann, AF., Wright-Patterson Air Force Base, Ohio, (Feb. 1969) AFML-TR-69-15.

45. M. H. Lewis and J. W. Martin, Acta Met. 11, 1207 (1963).

46. M. F. Ashby, Phil. Mag. 14, 1157 (1966).

47. F. J. Humphreys and J. W. Martin, Phil. Mag. 927 (1967).

48. E. R. Parker and V. F. Zackay, UCRL-18699, January 1969.

FIGURE CAPTIONS

Fig. 1. Ms temperature vs. annealing time for Type I alloy.

Fig. 2. X-ray diffraction profiles of the austenite after annealing. (Type I alloy).

Fig. 3. X-ray diffraction profiles of the LN cooled martensitic specimens. (Type I alloy).

Fig. 4. Volume fraction of martensite vs. annealing time for Type II alloys.

Fig. 5. Mechanical properties vs. annealing time for Type I alloys.

Fig. 6. $\Delta\sigma_{WH}$ (the difference between UTS and US) vs. annealing time for Type I alloys.

Fig. 7. $\Delta\sigma_{MT}$ (the difference between the yield stresses of austenite and corresponding martensite) vs. annealing time for Type I alloys.

Fig. 8. Mechanical properties vs. annealing temperatures for Type II alloys.

Fig. 9. Plot of tensile properties vs. annealing time (a) and $\Delta\sigma$ values vs. annealing time (b) for Type II alloys.

Fig. 10. Stress-strain curves for Type I and Type II alloys.

Fig. 11. Optical micrographs of LN cooled Type I alloy (a) and annealed at 600°C/7 hrs and LN cooled specimen (b).

Fig. 12. Optical micrographs of strain induced martensite in Type I alloys.

Fig. 13. Electron micrographs show the unannealed (a) and (b) annealed austenitic structures (Type I).

Fig. 14. Electron micrographs of LN cooled martensite structures (Type I).

Fig. 15. Bright field (a) and dark field images (b), (c) of 600°C/7 hrs annealed and LN cooled martensitic structures (Type I).

Fig. 16. Bright field (a) and dark field (b), (c) images show the presence

Fig. 30. Structures of strain-induced martensite (Type I).

Fig. 31. Structures of strain-induced martensite (Type I).

Fig. 32. Structures of strain-induced martensite, showing the needle shaped morphology of martensite crystals (Type I).

Fig. 33. Scanning electron micrographs of tensile broken specimens of (a), (b) austenite and (c), (d) LN cooled specimens (Type I).

Fig. 34. Scanning electron micrographs of tensile broken specimen of austenitic Type II alloys.

Fig. 35. Scanning electron micrographs of tensile broken specimens of 500°C/1 hr alloy showing the mixed mode of fracture, namely, intergranular and transgranular (Type II).

Fig. 36. Scanning electron micrograph of the LN cooled, unannealed Type II alloy.

Fig. 37. Scanning electron micrographs of the 500°C/3 hr and LN cooled Type II alloy.

Fig. 38. Schematic description of the martensitic transformation of a dispersion-hardened austenite.

Fig. 39. Plot of yield strength vs. volume fraction of martensite of Type II alloy.

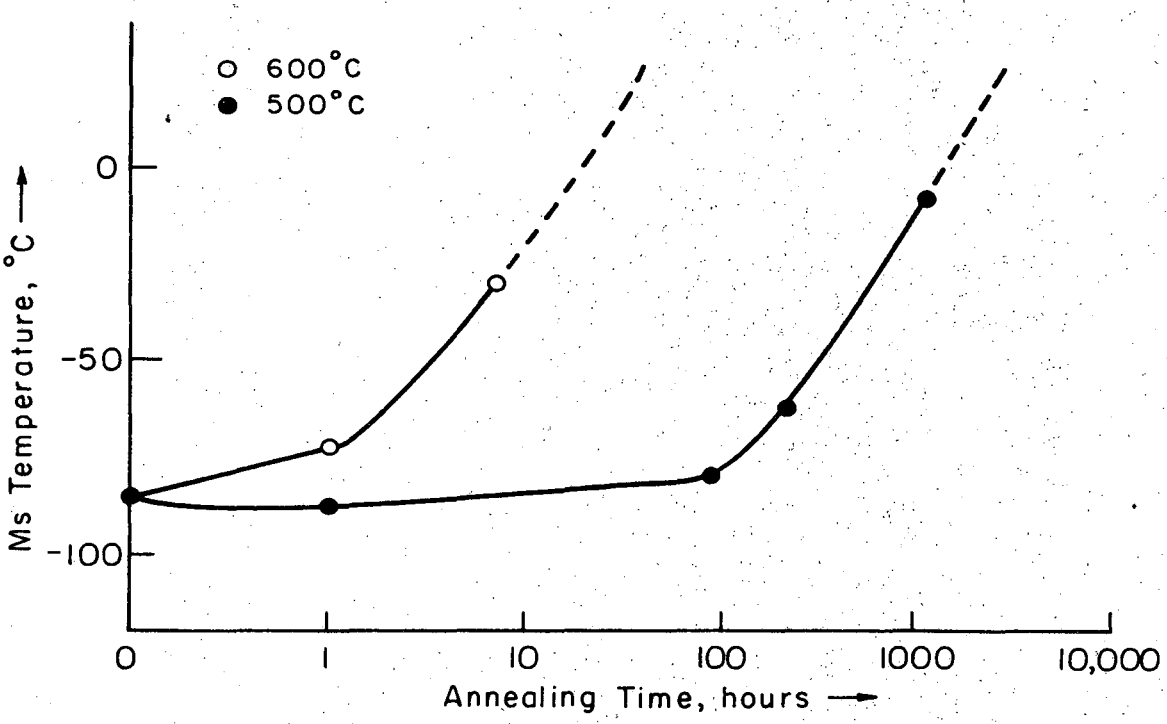
600°C
500°C
0
-50
-100
Ms Temperature, °C
0
1
10
100
1000
10,000
Annealing Time, hours
XBL 704-662

Fig. 1

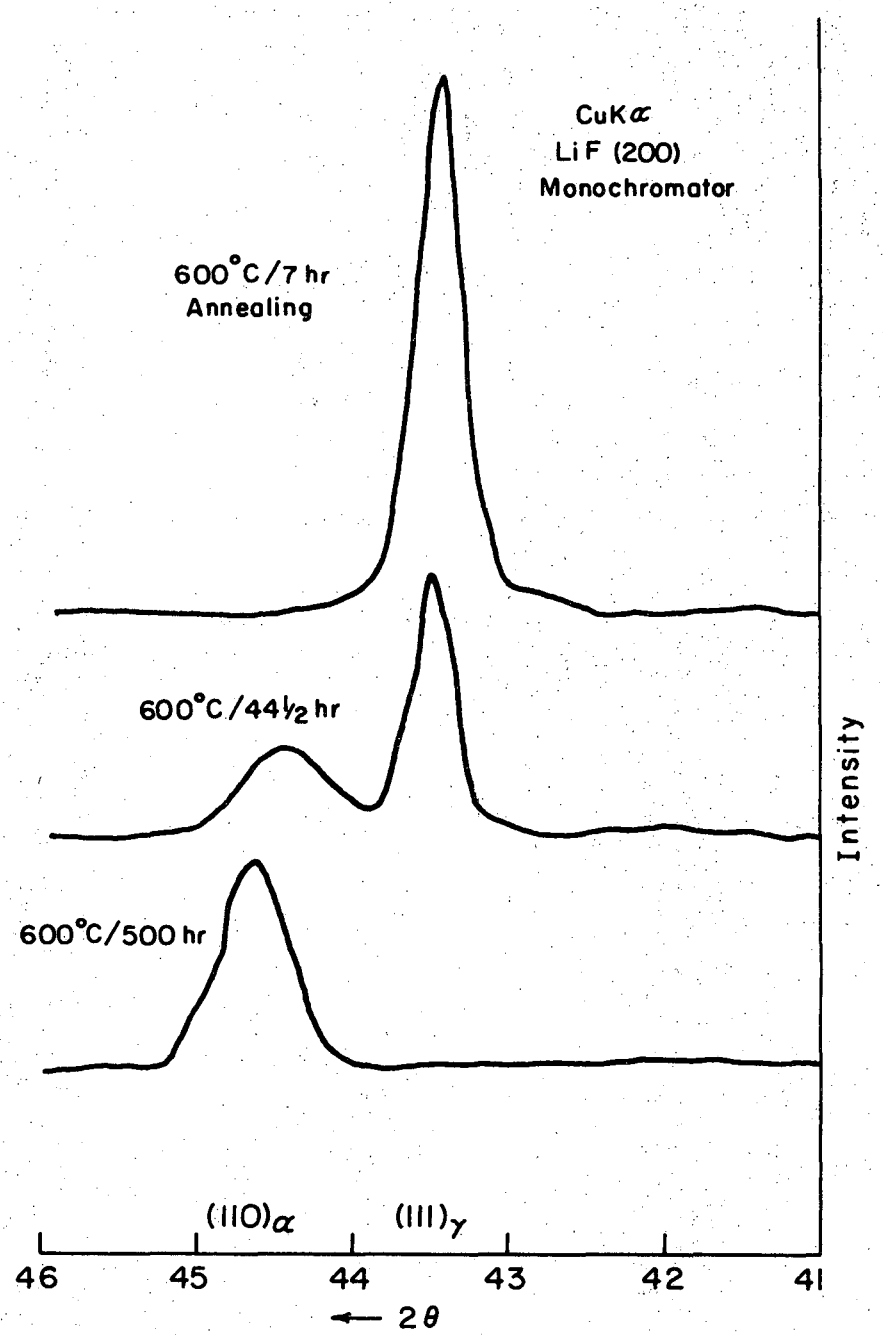

XBL 704-665

Fig. 2

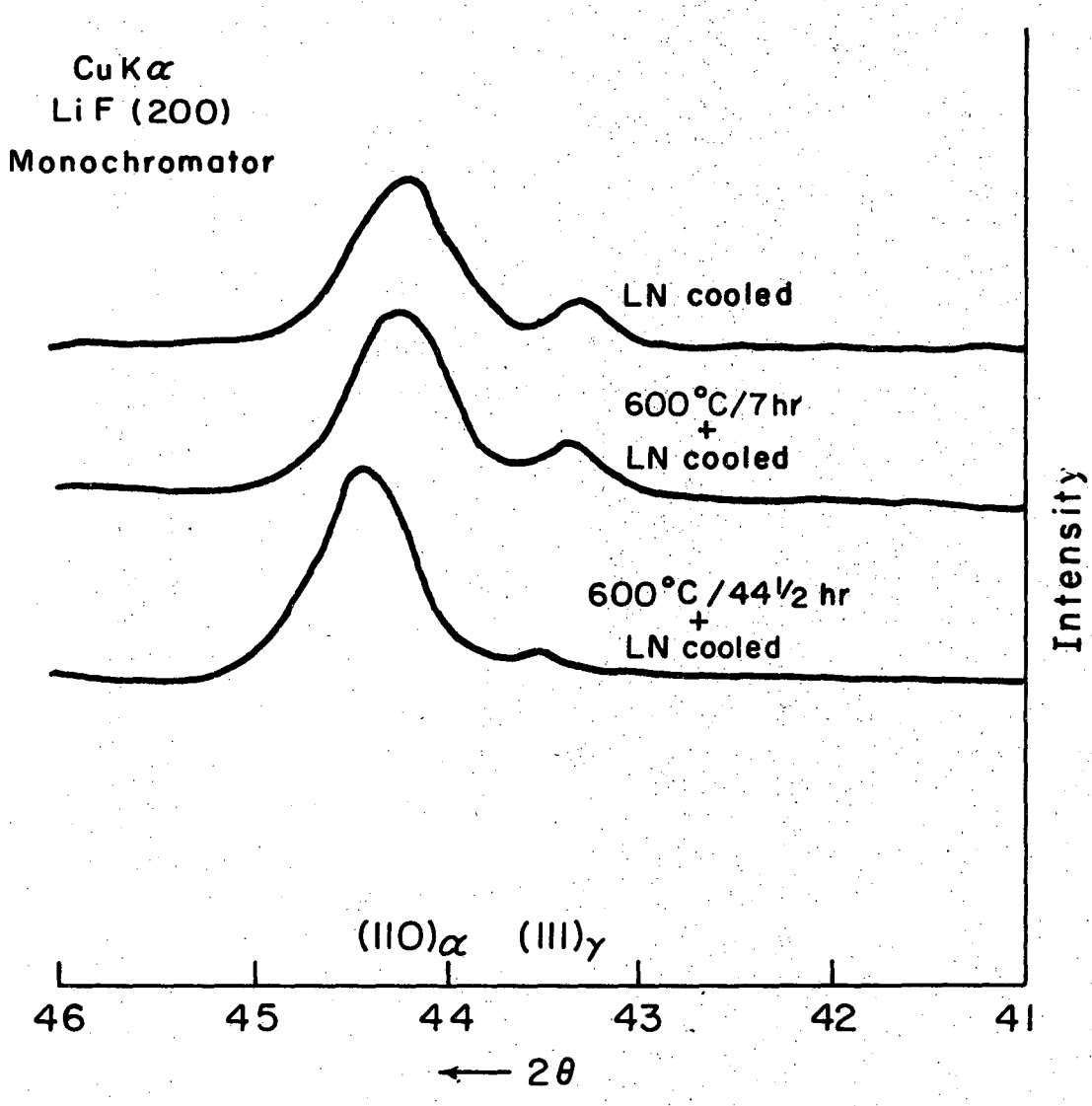

XBL 704-663

Fig. 3

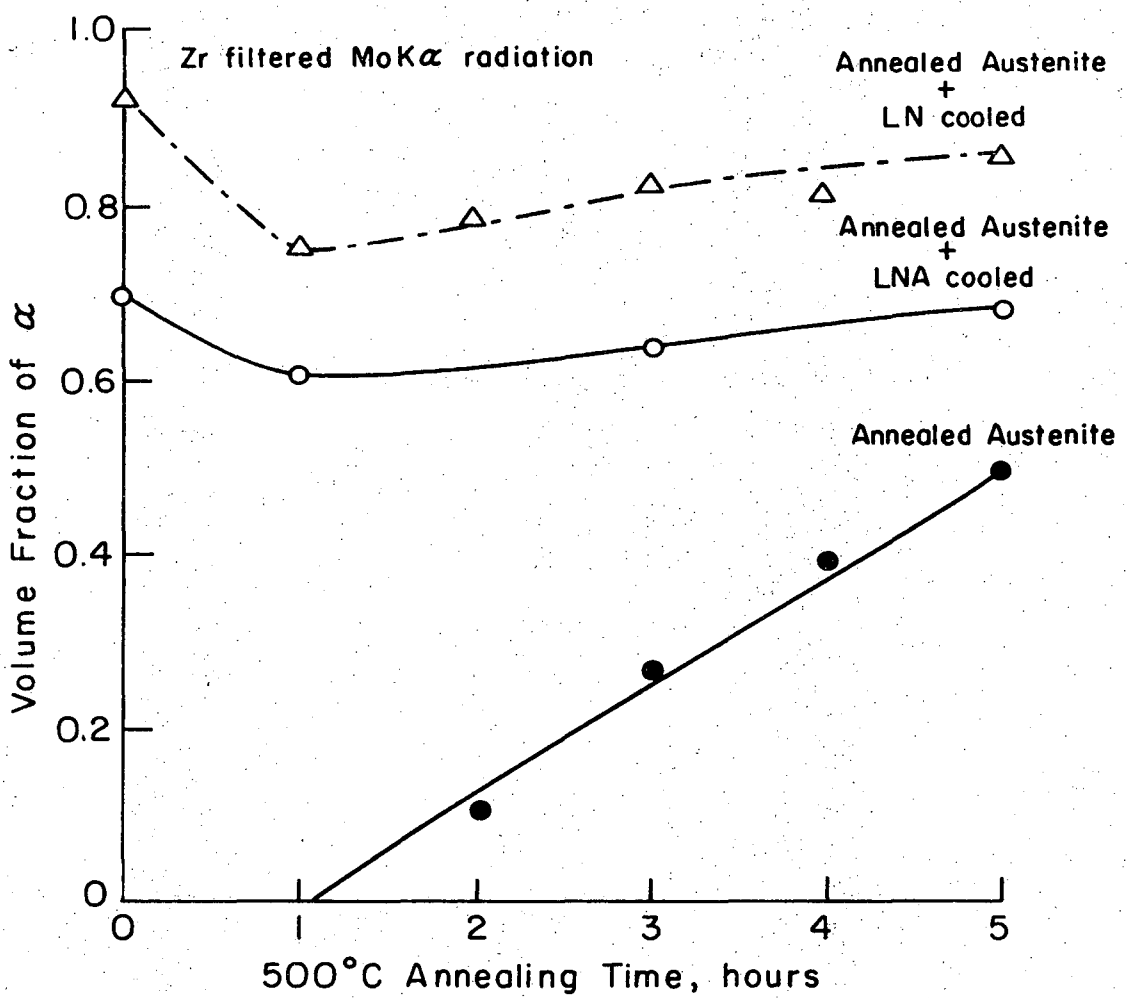

XBL 704-664

Fig. 4

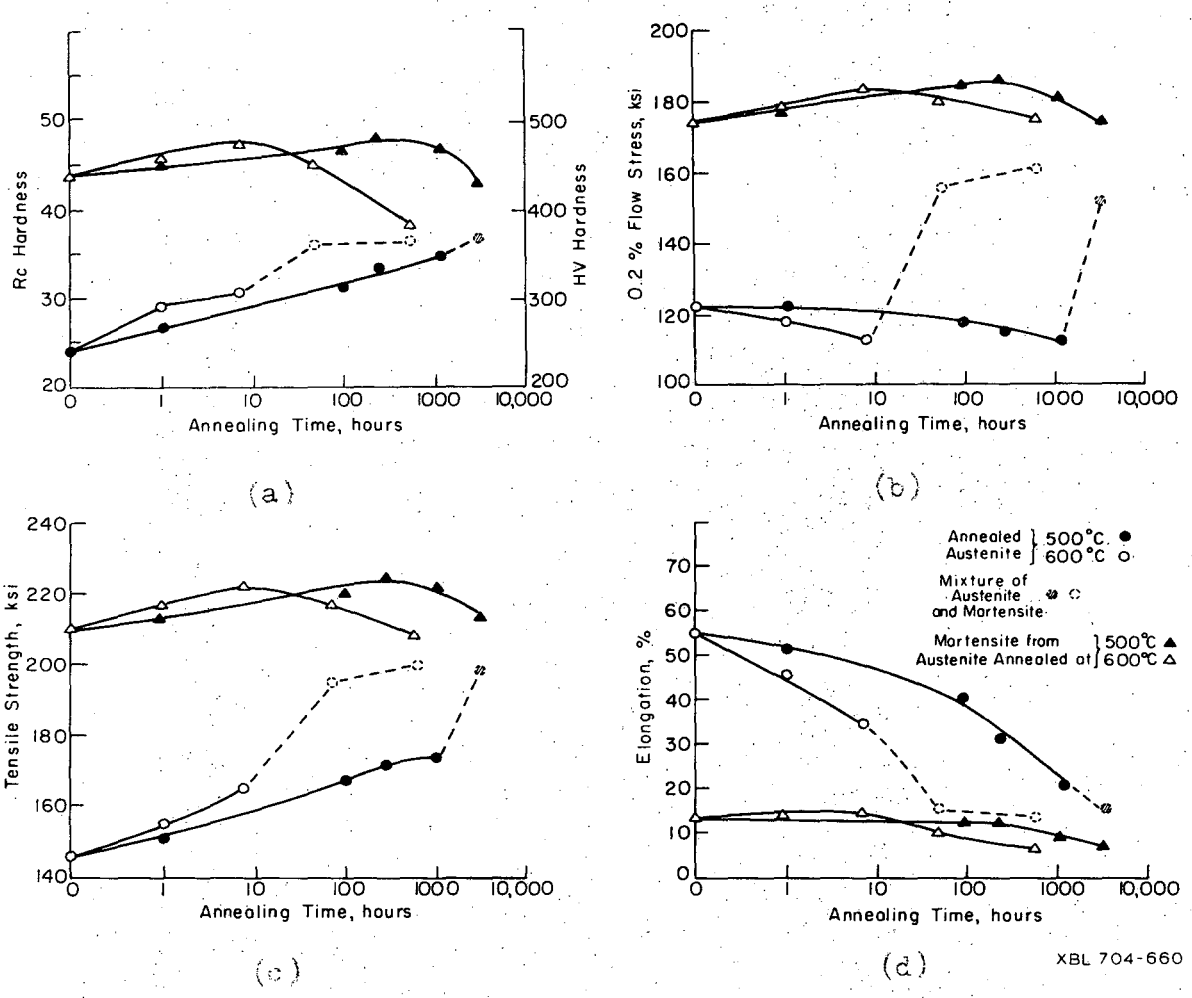
Rc Hardness
HV Hardness
Annealing Time, hours
(a)
0.2 % Flow Stress, ksi
Annealing Time, hours
(b)
Tensile Strength, ksi
Annealing Time, hours
(c)
Annealed Austenite 500°C ● 600°C ○
Mixture of Austenite and Martensite ◍ ◌
Martensite from Austenite Annealed at 500°C ▲ 600°C △
Elongation, %
Annealing Time, hours
(d)
XBL 704-660

Fig. 5

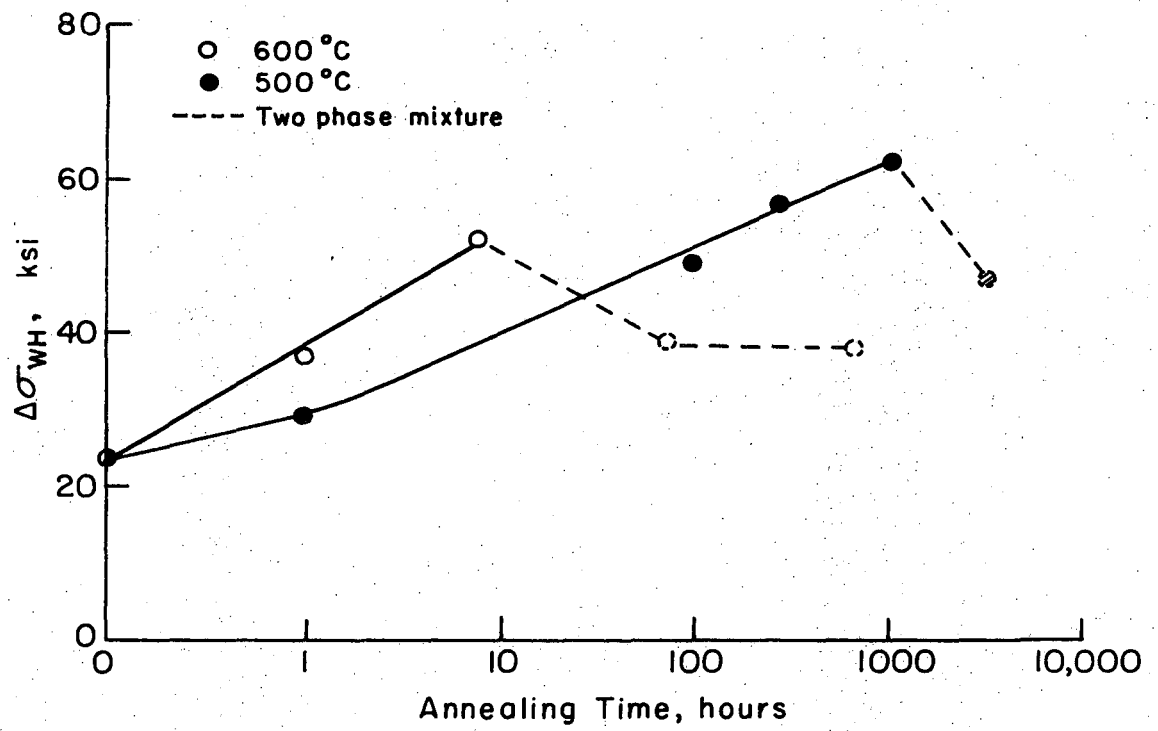
80
60
40
20
0
$\Delta\sigma_{WH}$, ksi
600°C
500°C
Two phase mixture
0
1
10
100
1000
10,000
Annealing Time, hours
XBL 704-661

Fig. 6

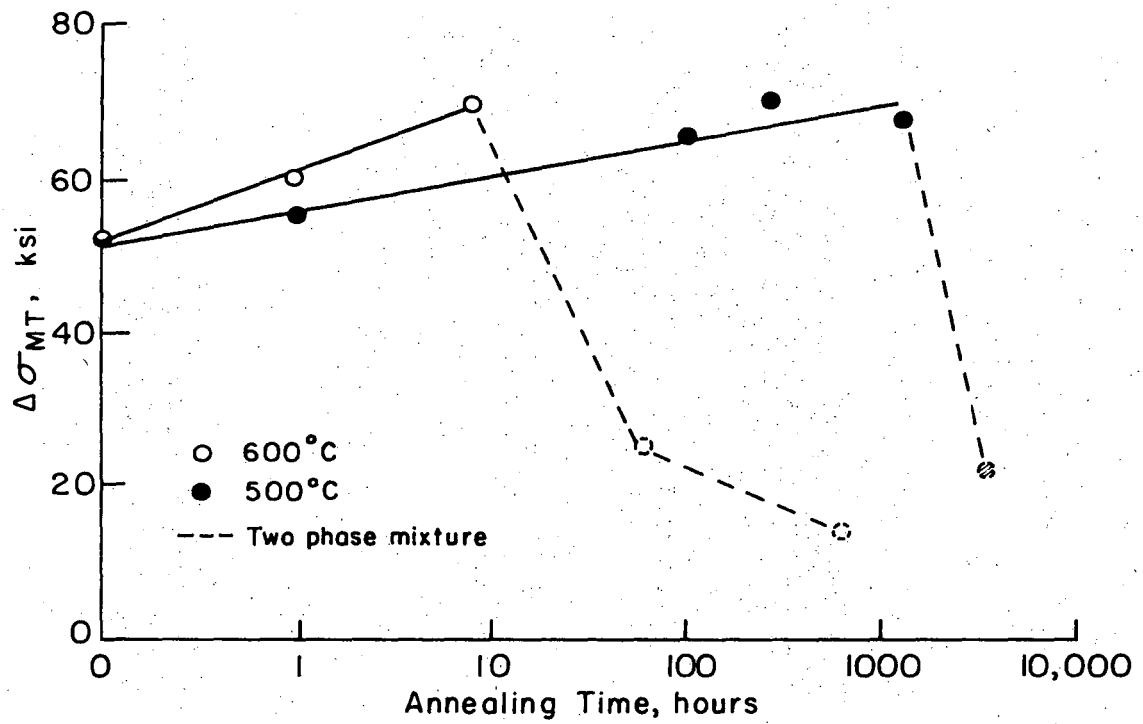

XBL 704-669

Fig. 7

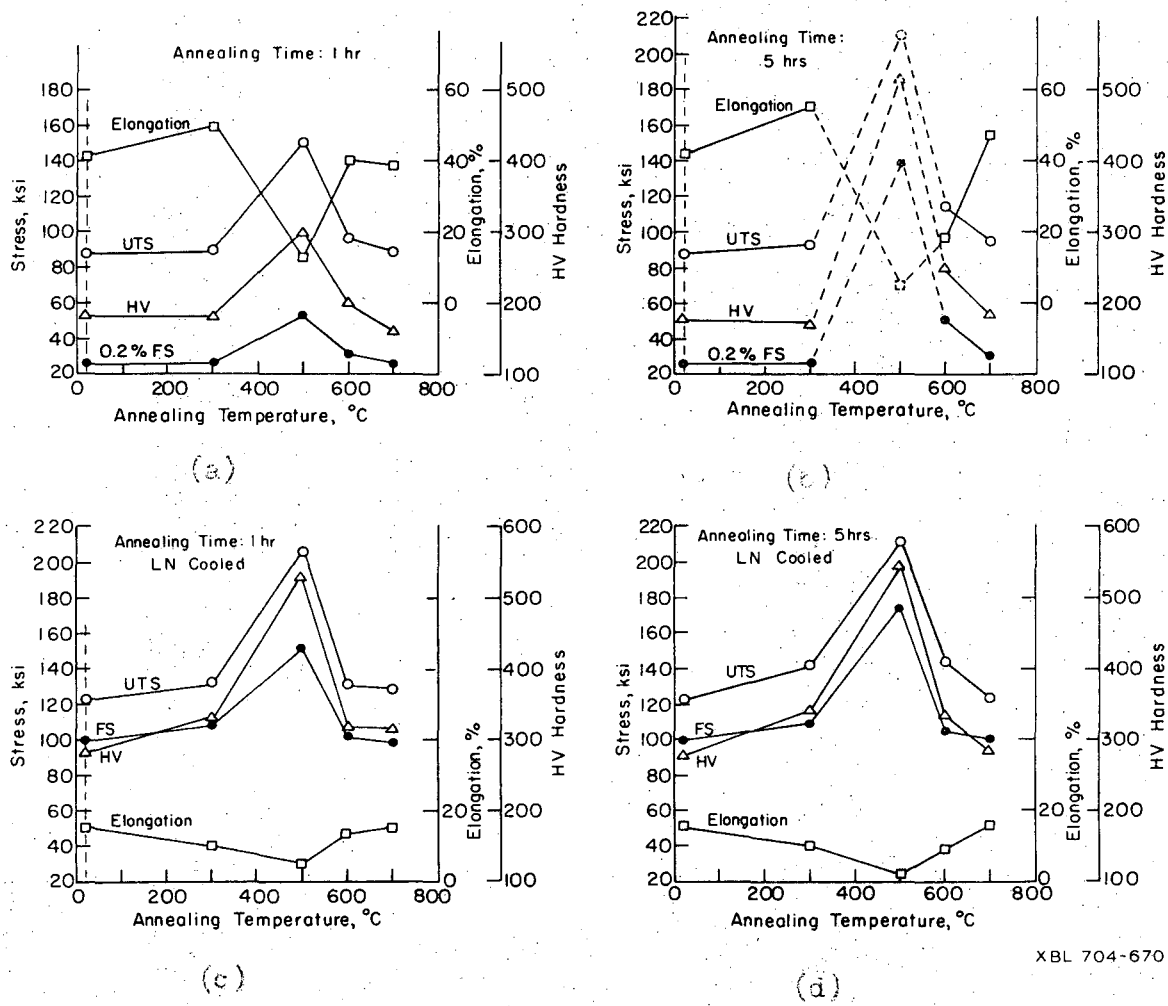
Annealing Time: 1 hr
Elongation
UTS
HV
0.2% FS
Stress, ksi
Elongation, %
HV Hardness
Annealing Temperature, °C
(a)
Annealing Time: 5 hrs
(b)
Annealing Time: 1 hr
LN Cooled
FS
(c)
Annealing Time: 5hrs
(d)
XBL 704-670

Fig. 8

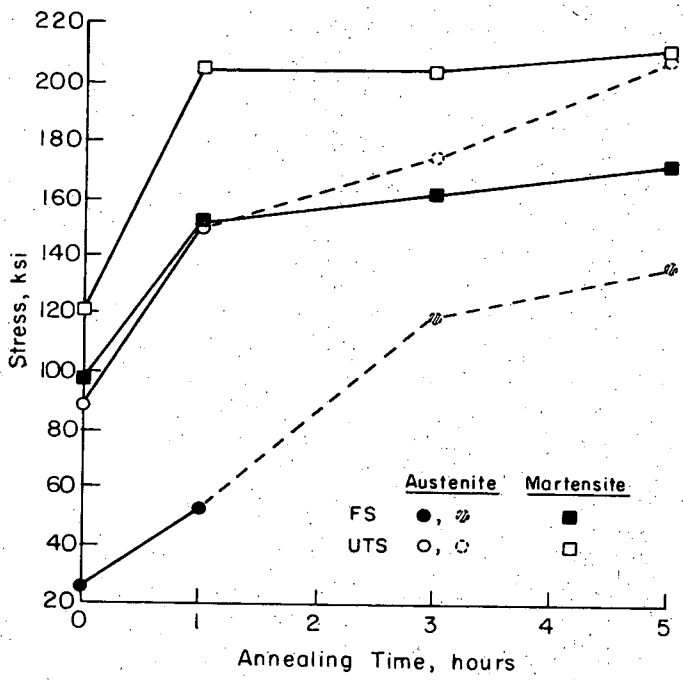

Fig. 9a (a)

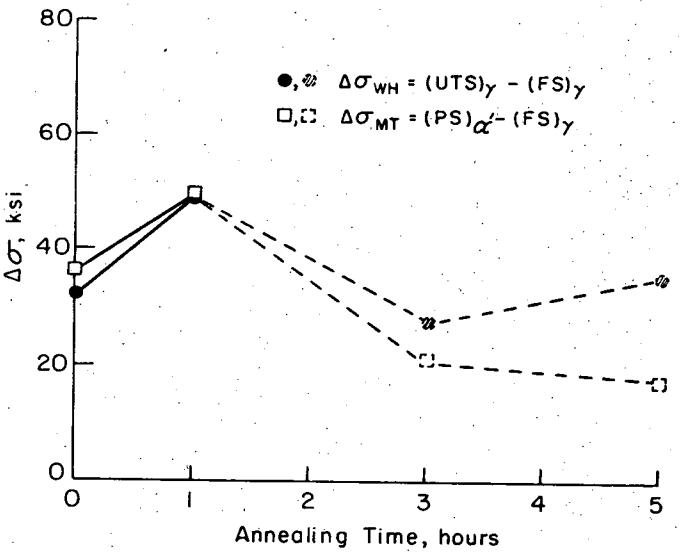

(b) XBL 704-659

Fig. 9

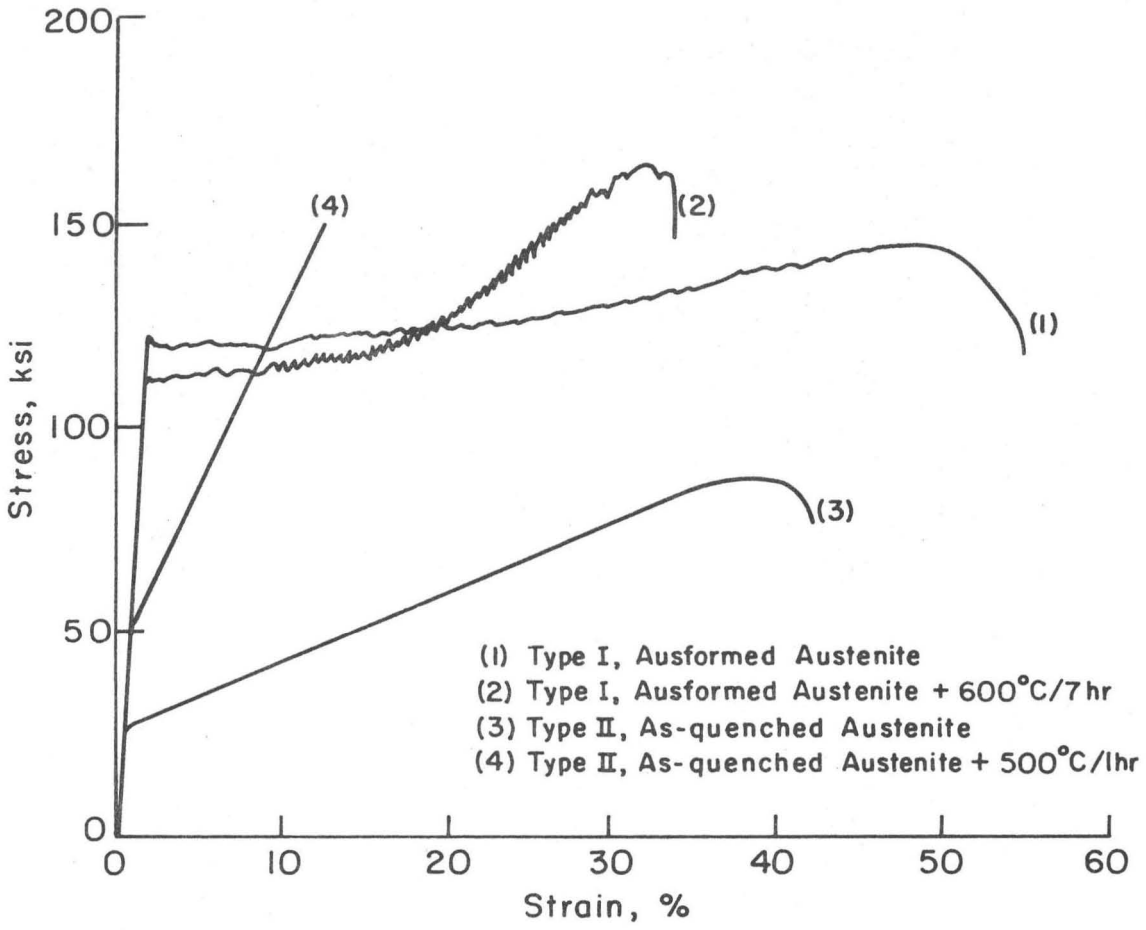

XBL 704-668

Fig. 10

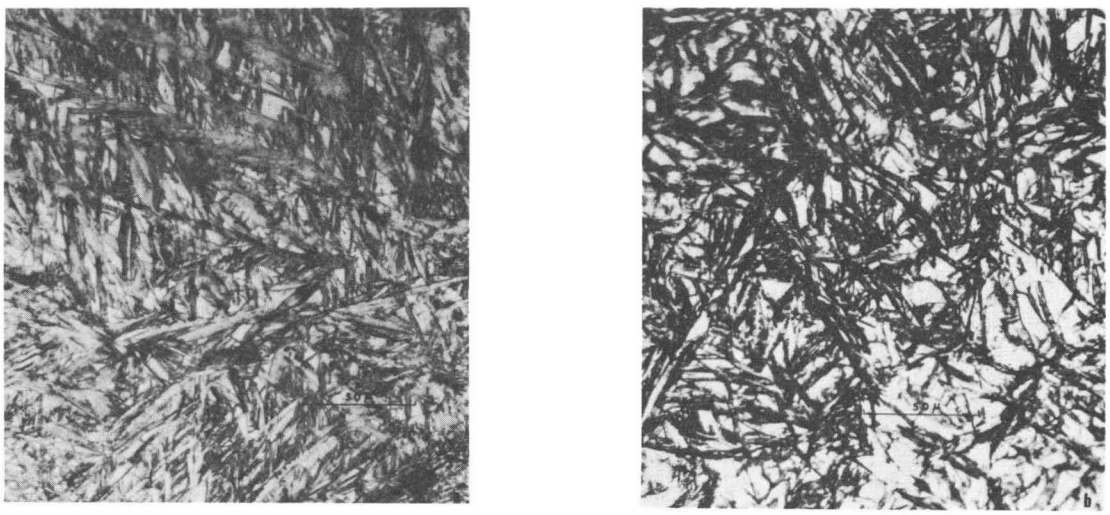

XBB 704-1556

Fig. 11

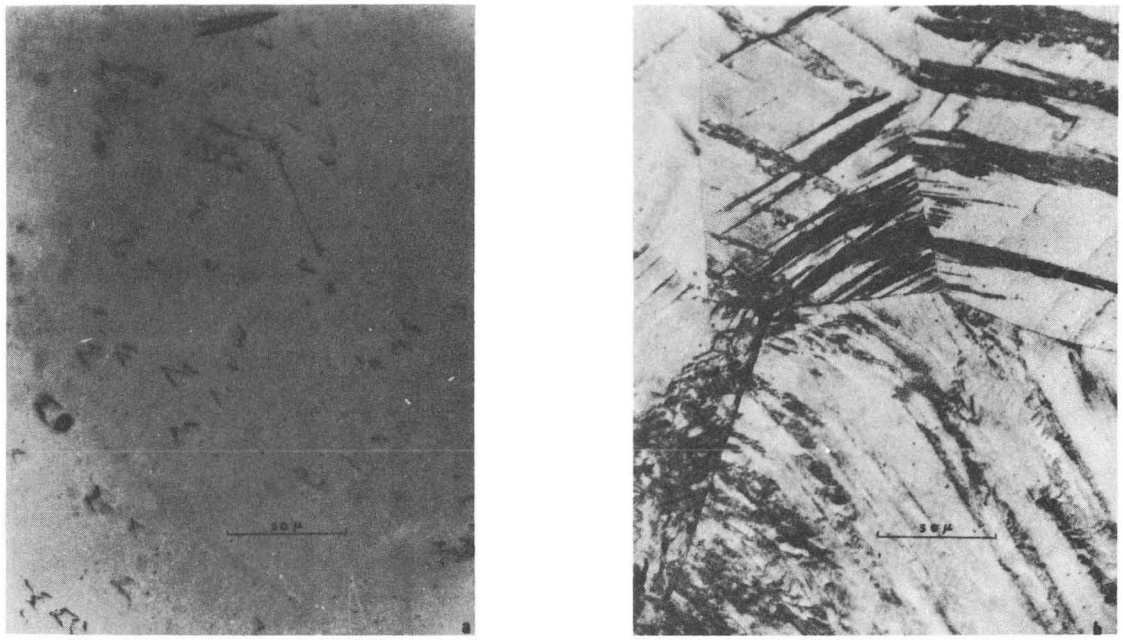

XBB 704-1557

Fig. 12

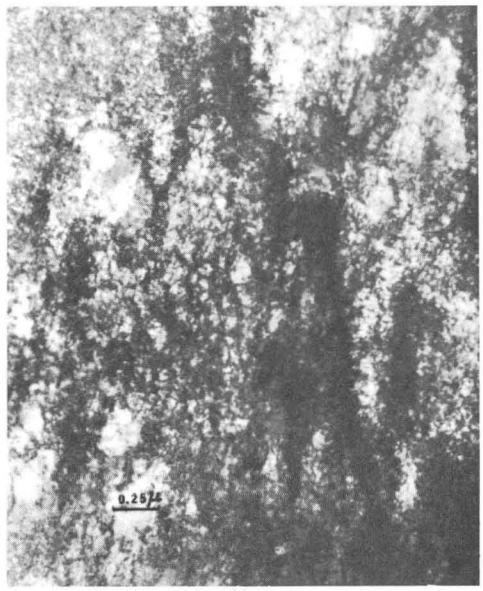

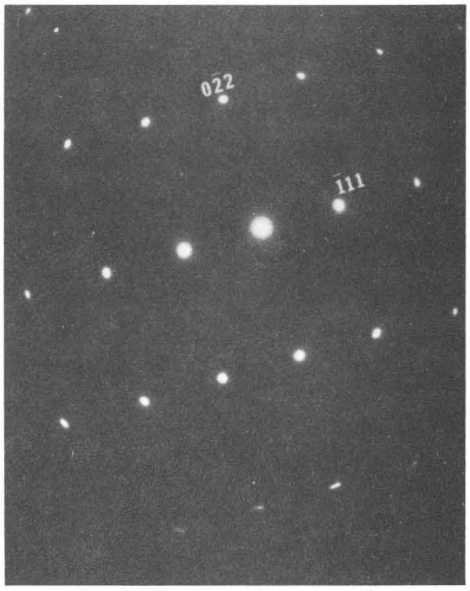

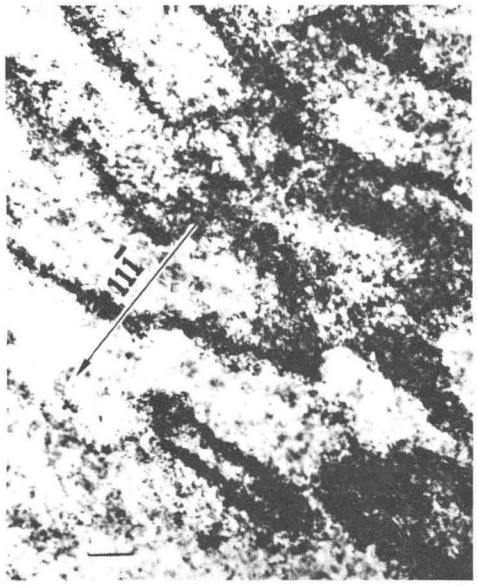

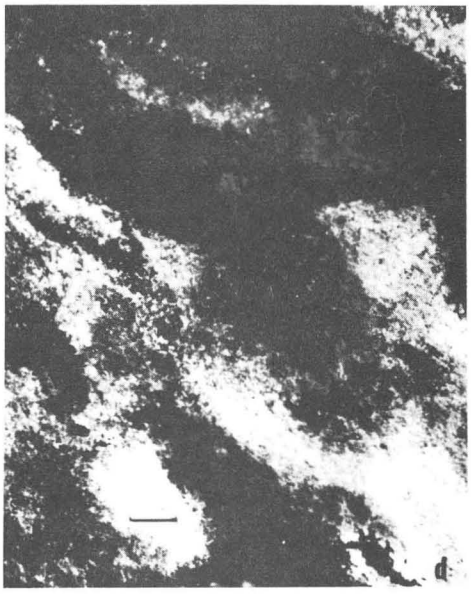

XBB 704-1543

Fig. 13

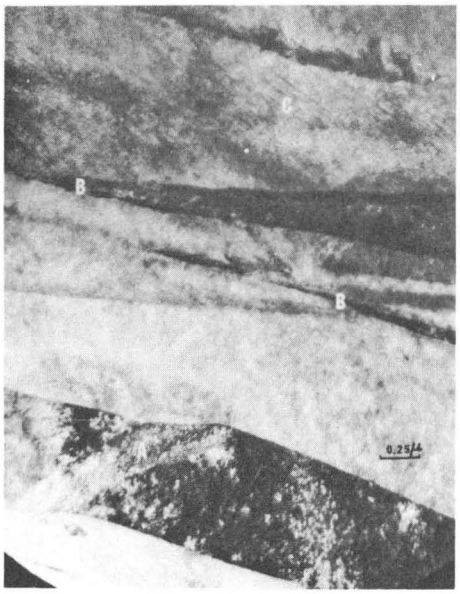

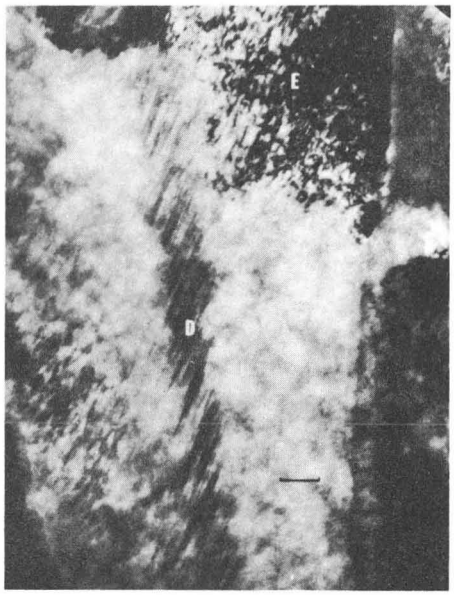

XBB 704-1559

Fig. 14

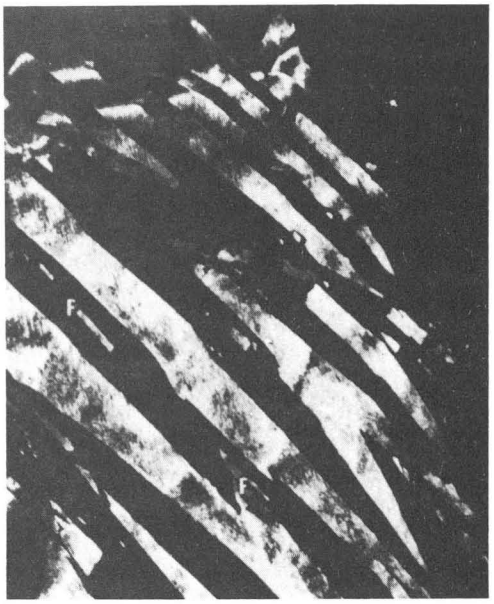

XBB 704-1547

Fig. 15

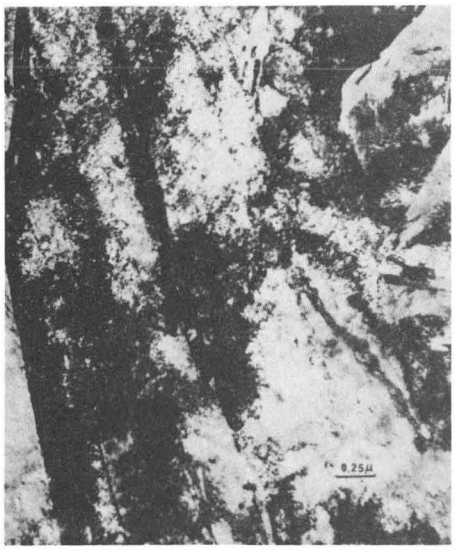

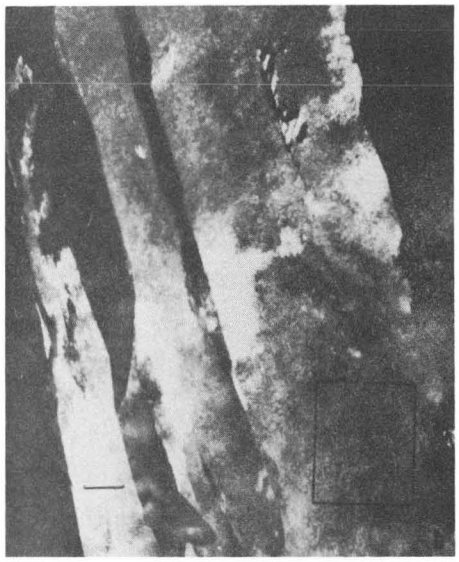

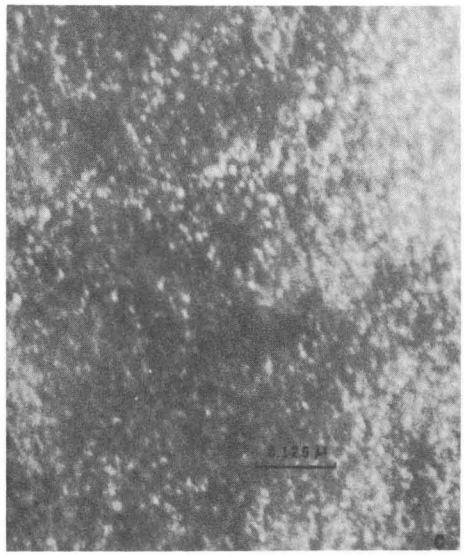

XBB 704-1544

Fig. 16

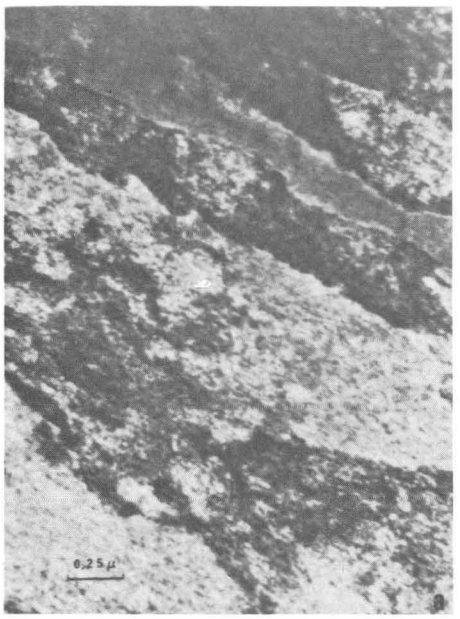

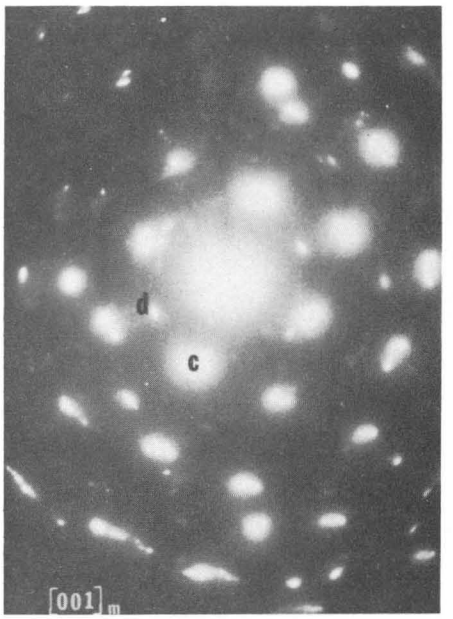

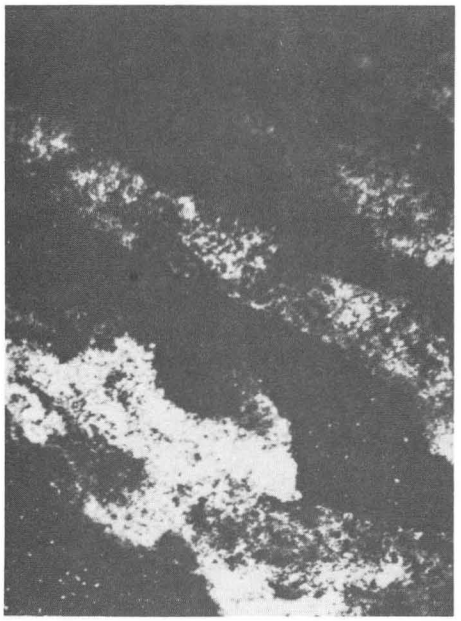

XBB 704-1541

Fig. 17

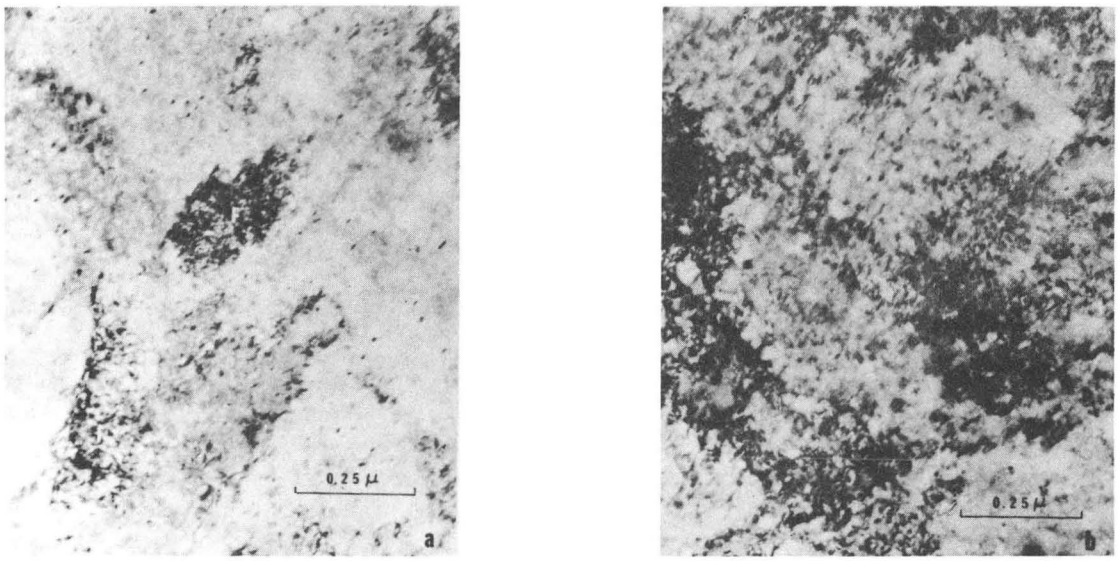

XBB 704-1555

Fig. 18

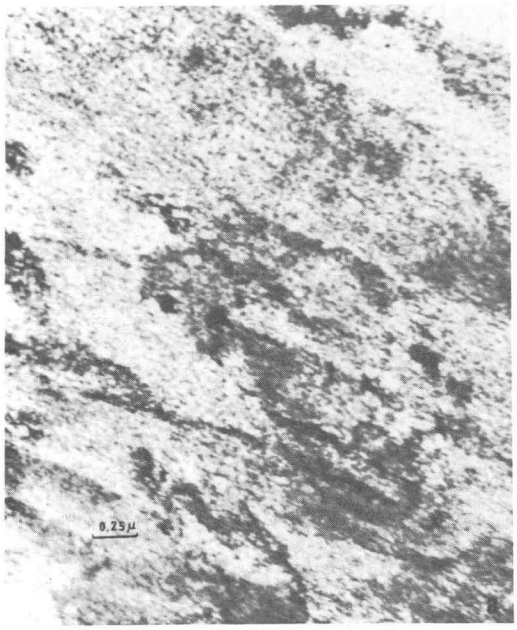

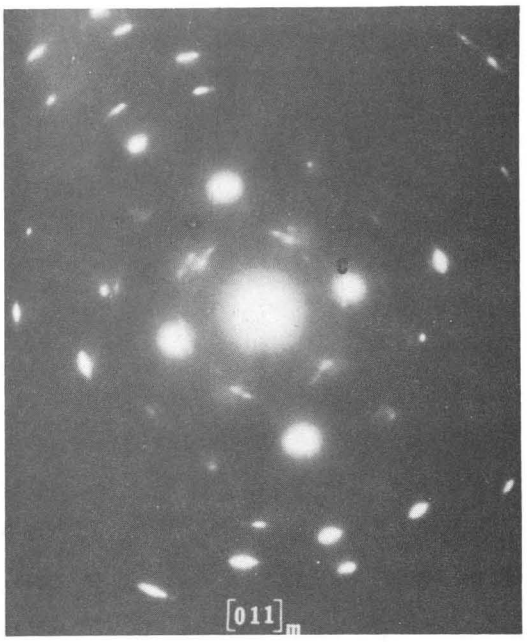

XBB 704-1542

Fig. 19

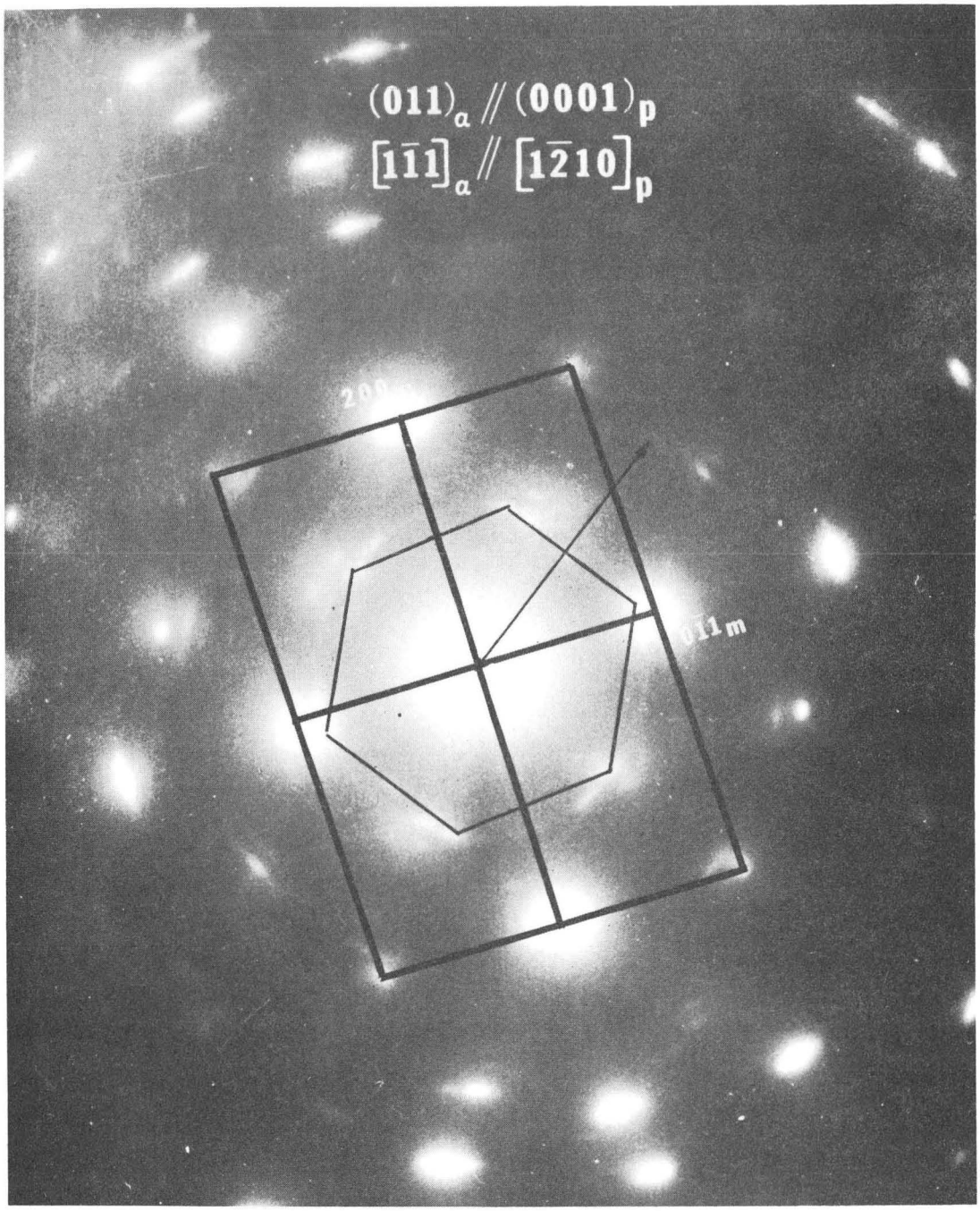

XBB 704-1550

Fig. 20

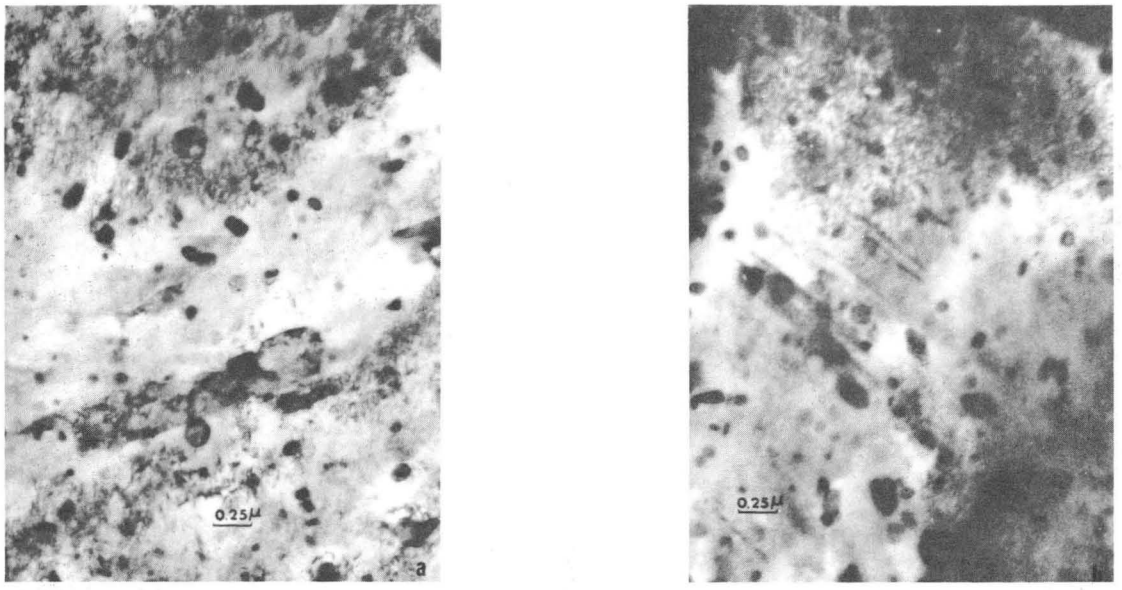

XBB 704-1554

Fig. 21

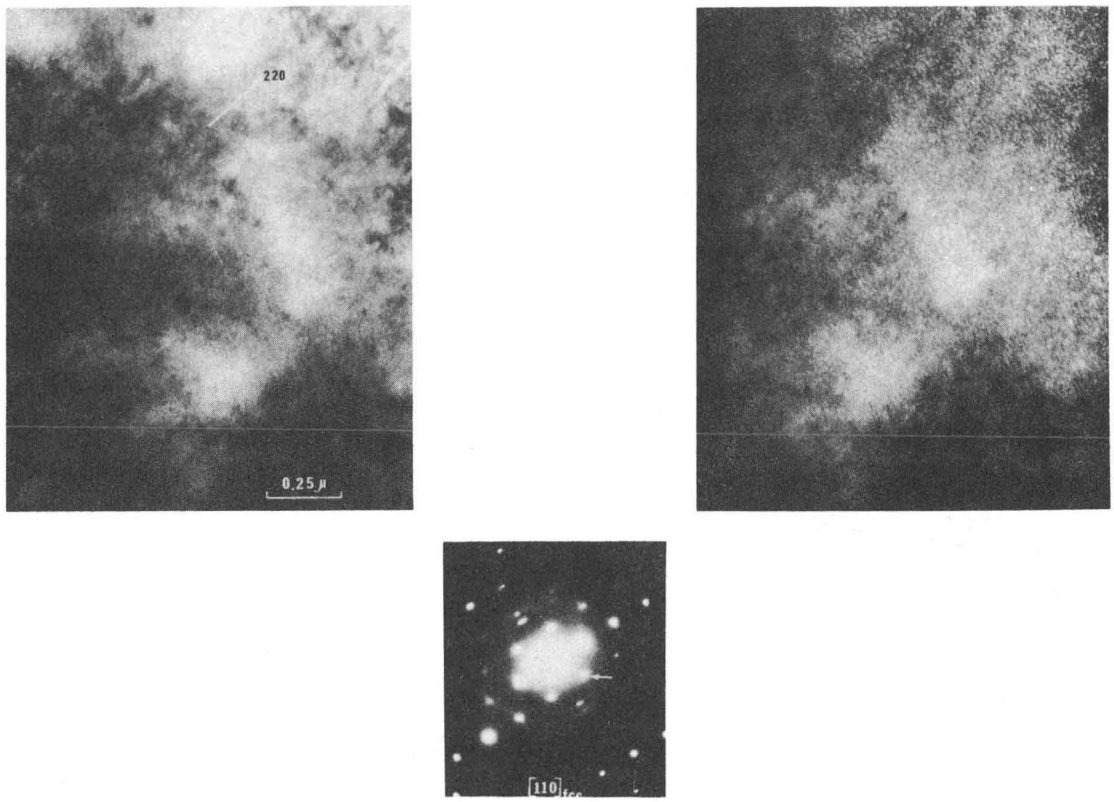

XBB 704-1558

Fig. 22

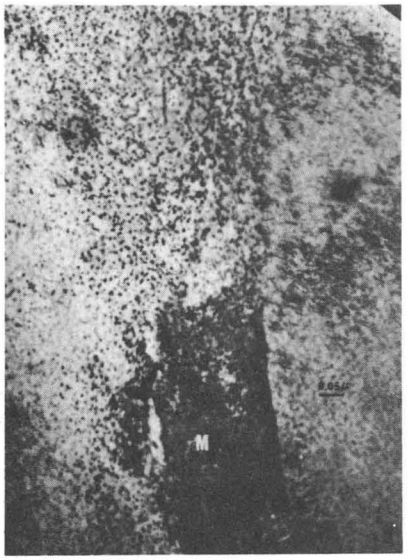

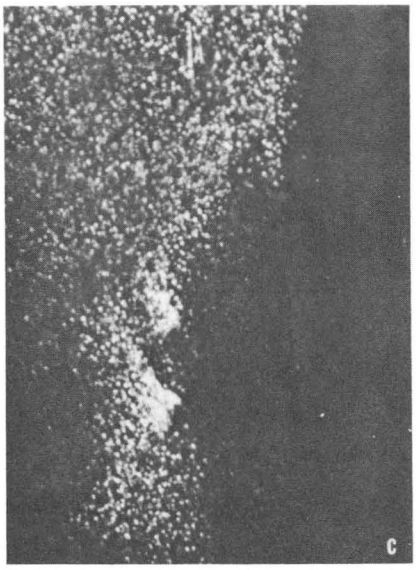

XBB 704-1553

Fig. 23

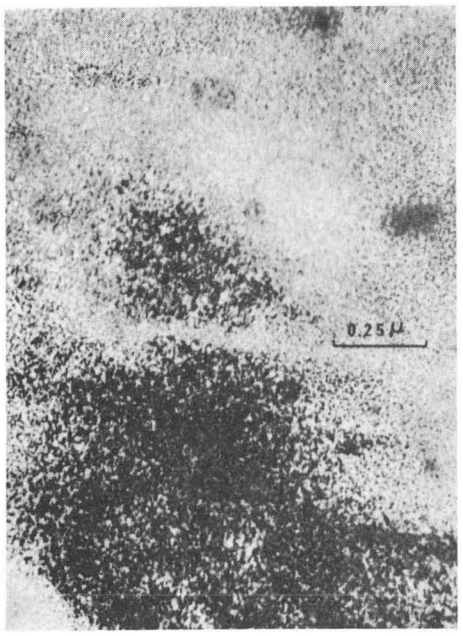

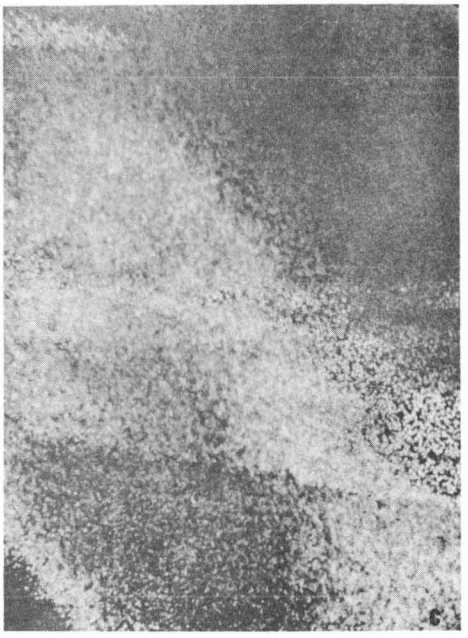

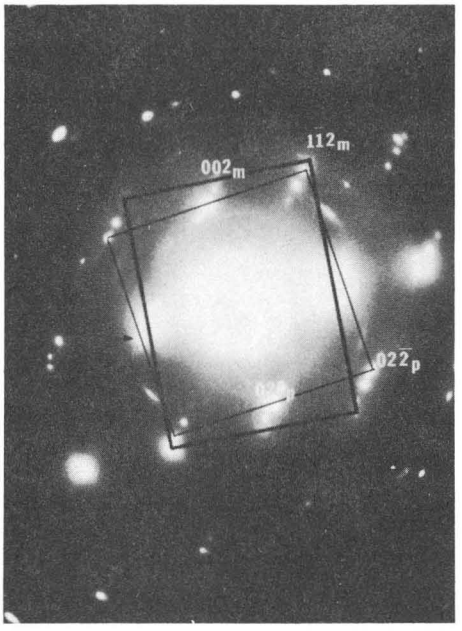

XBB 704-1548

Fig. 24

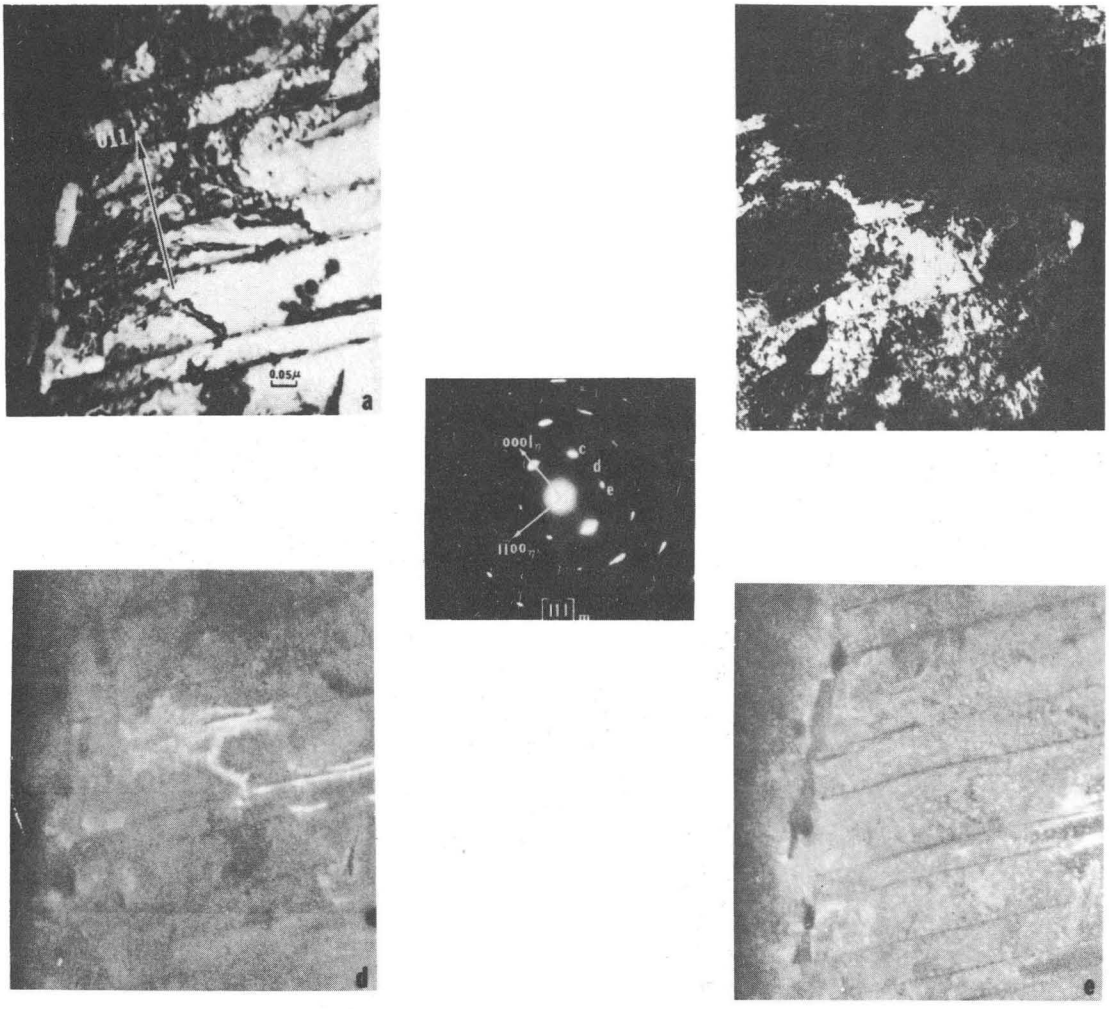

XBB 704-1552

Fig. 25

XBB 704-1561

Fig. 26

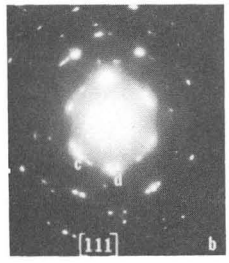

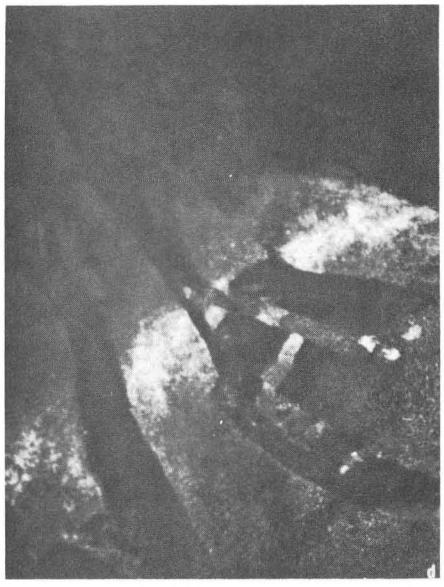

XBB 704-1539

Fig. 27

XBB 704-1549

Fig. 28

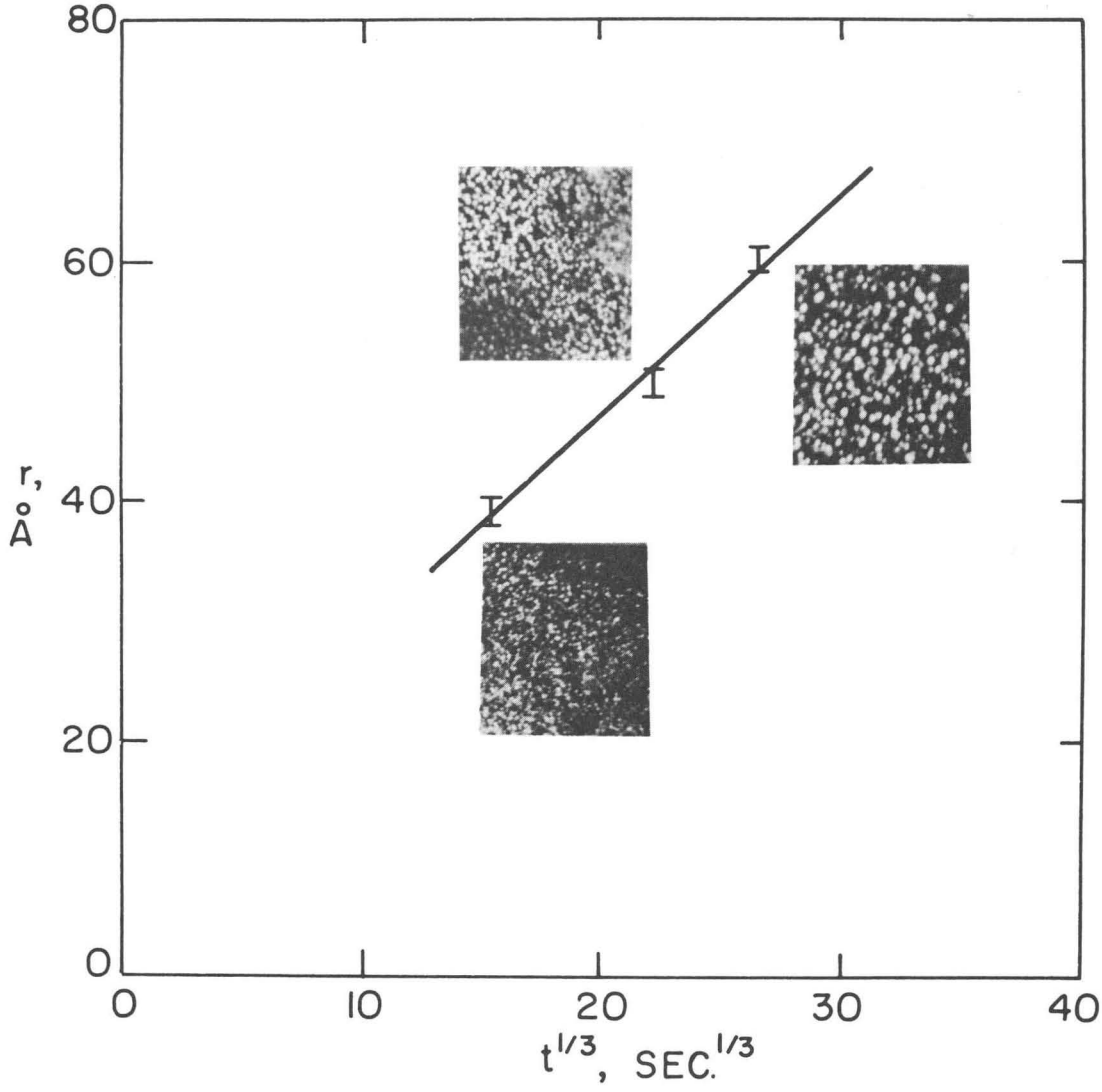

XBB 704-1551

Fig. 29

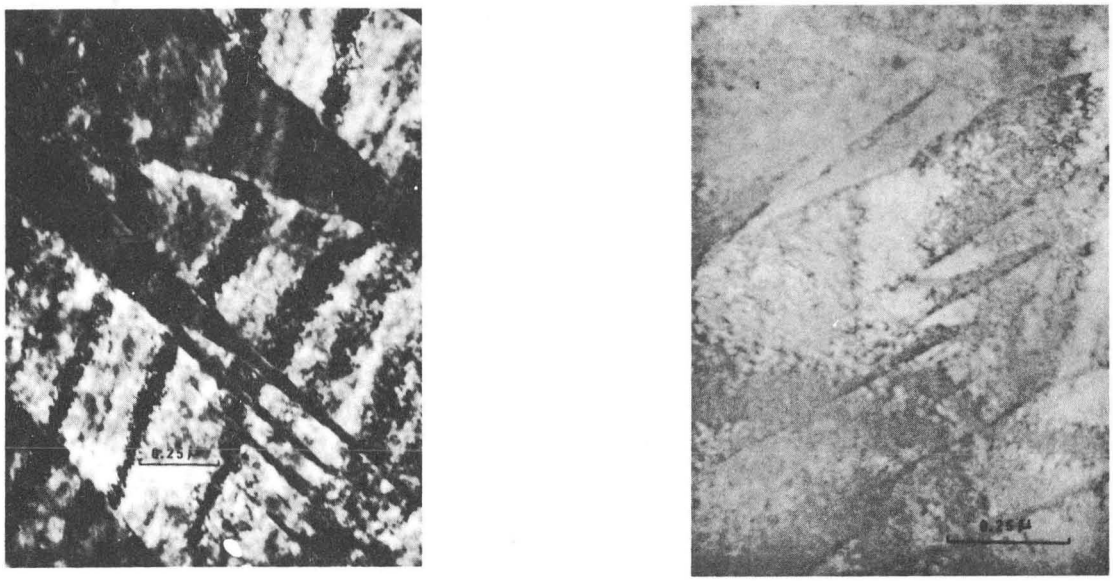

XBB 704-1562

Fig. 30

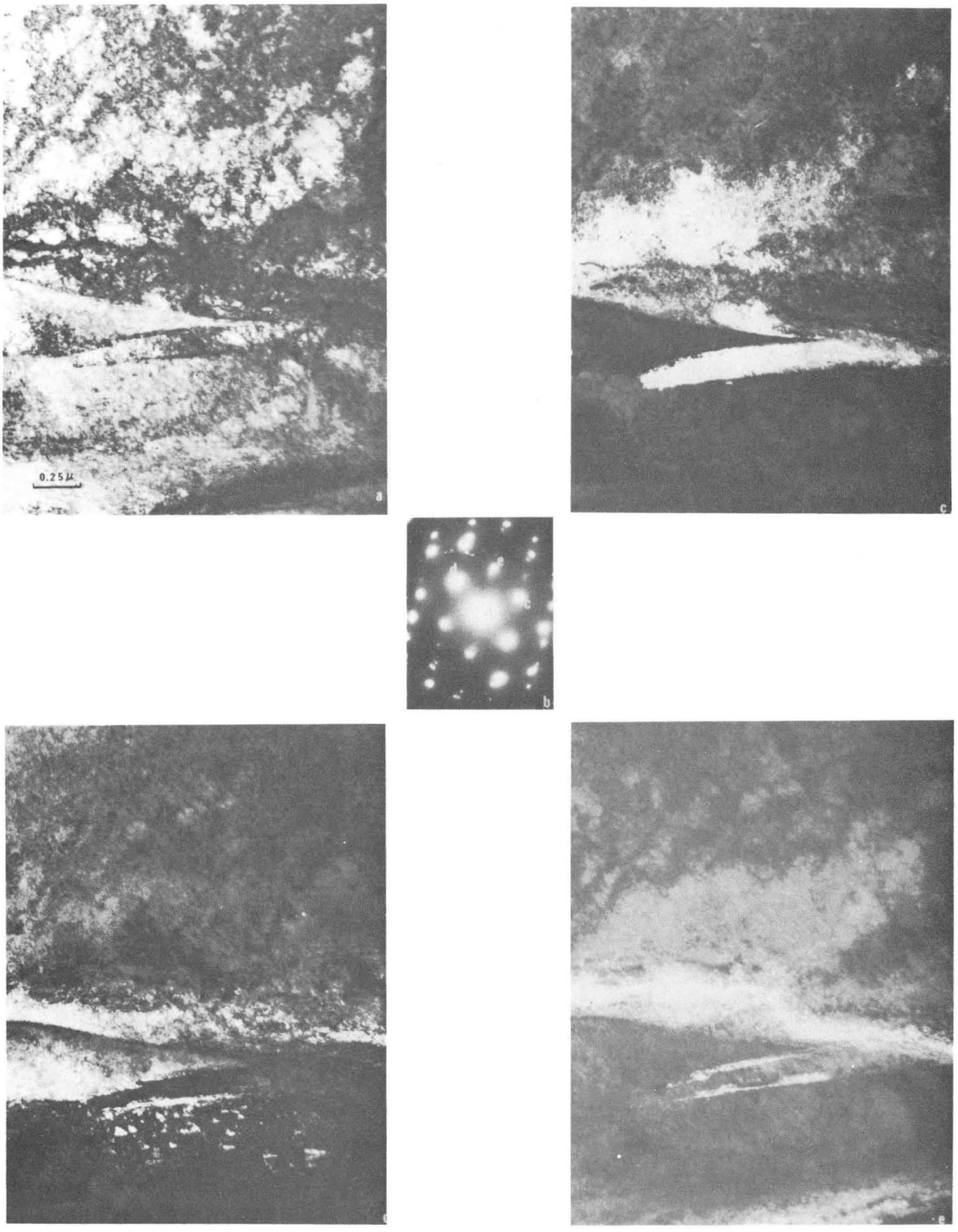

XBB 704-1538

Fig. 31

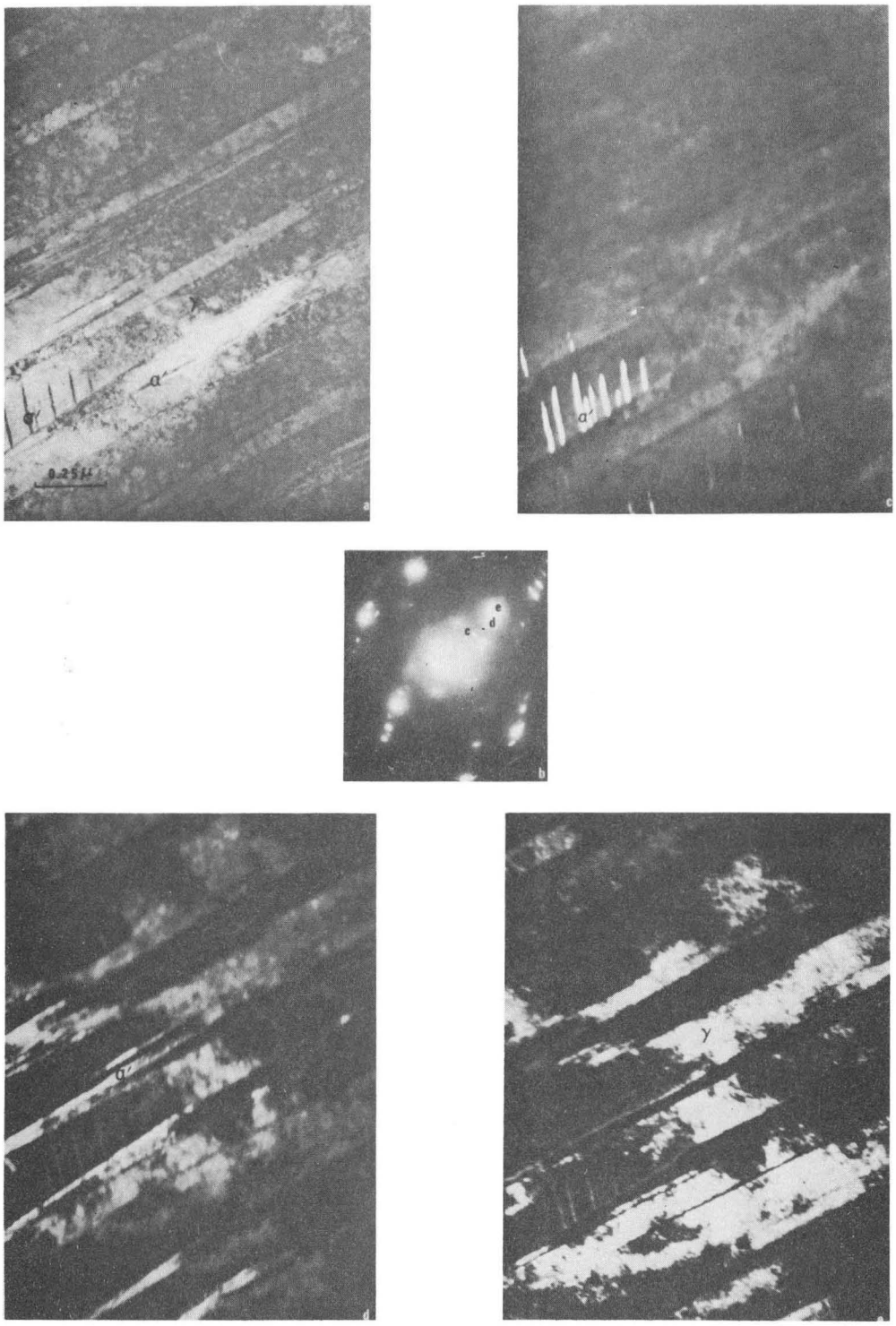

XBB 704-1537

Fig. 32

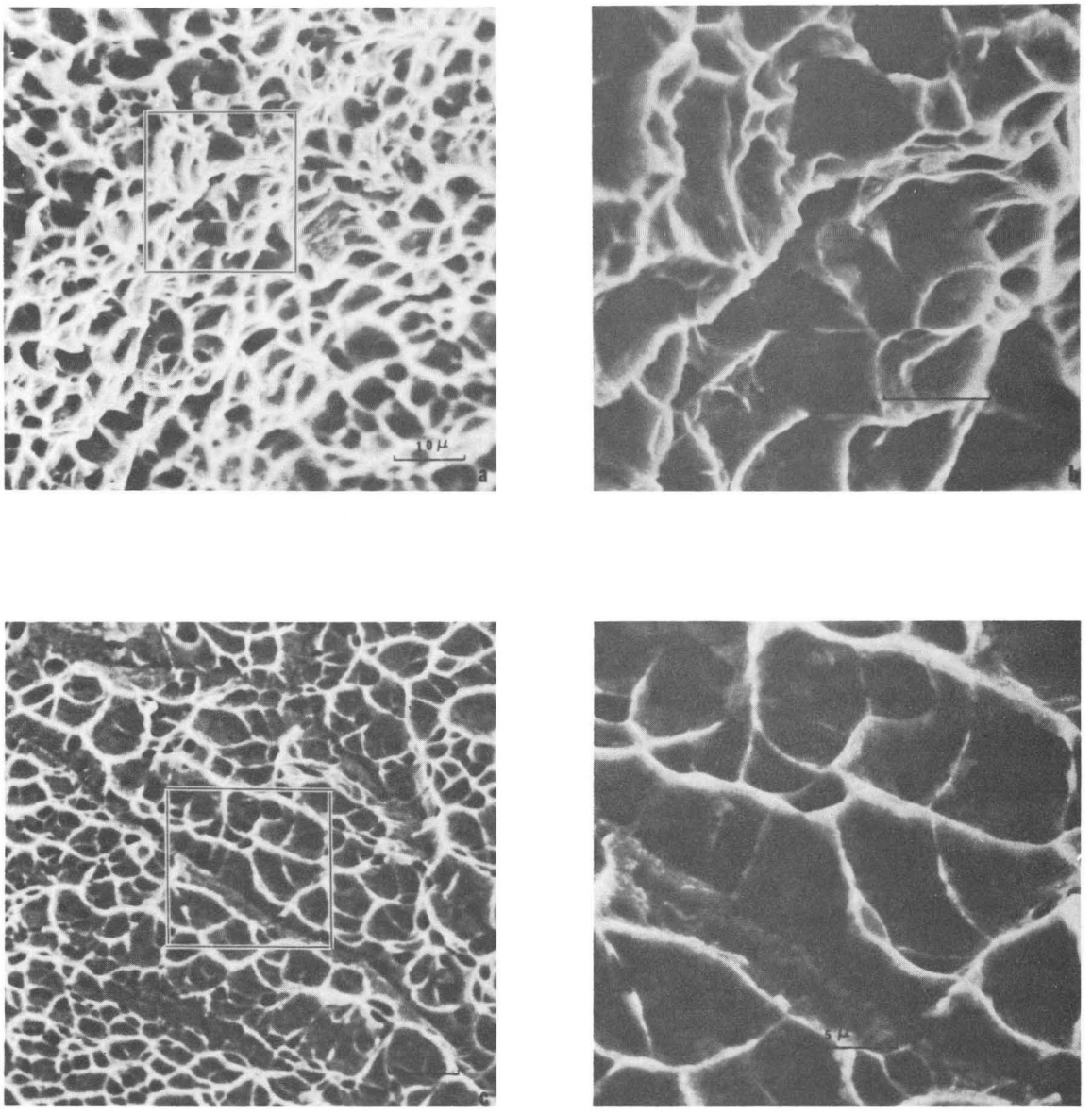

XBB 704-1540

Fig. 33

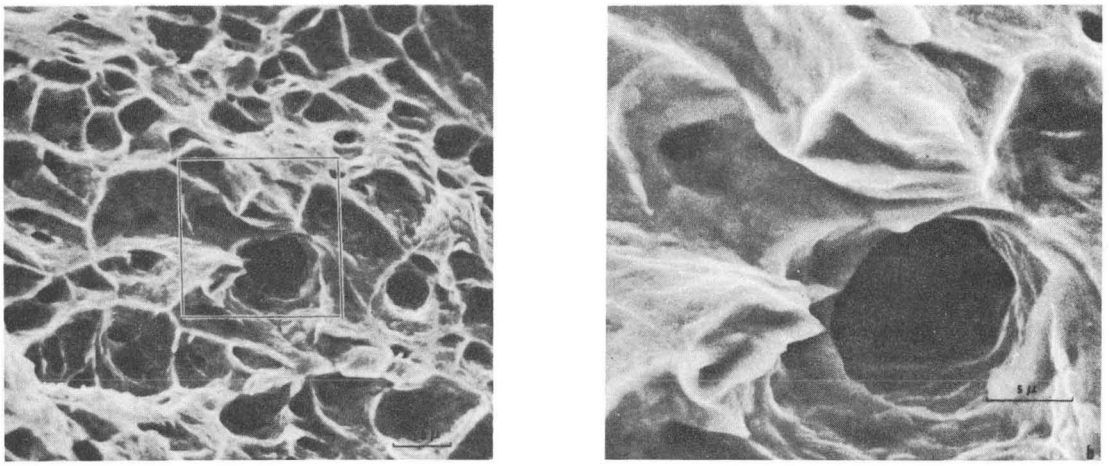

XBB 704-1560

Fig. 34

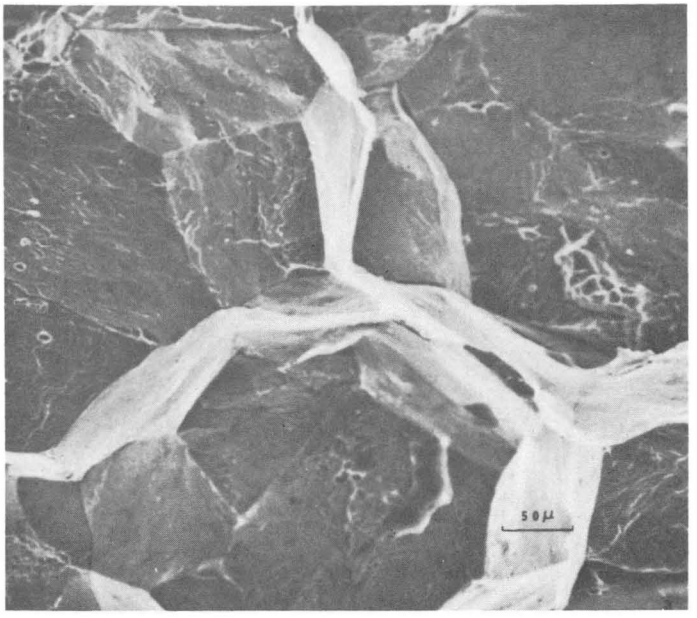

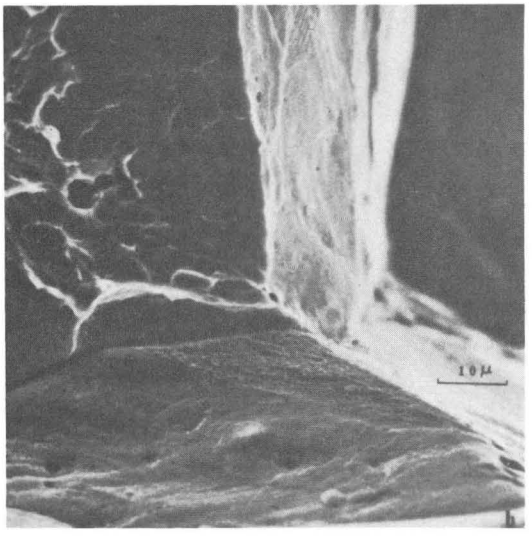

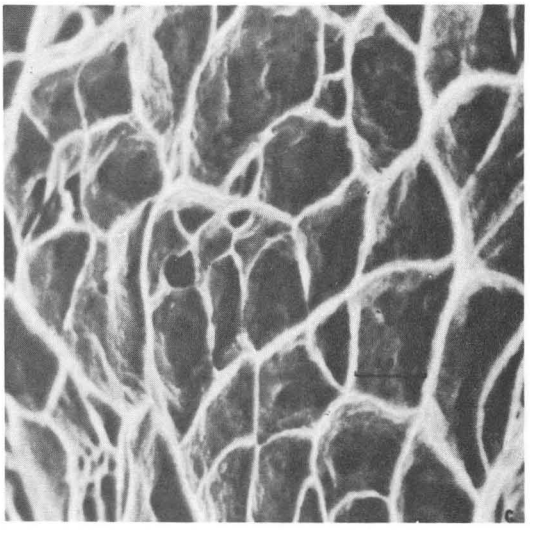

XBB 704-1546

Fig. 35

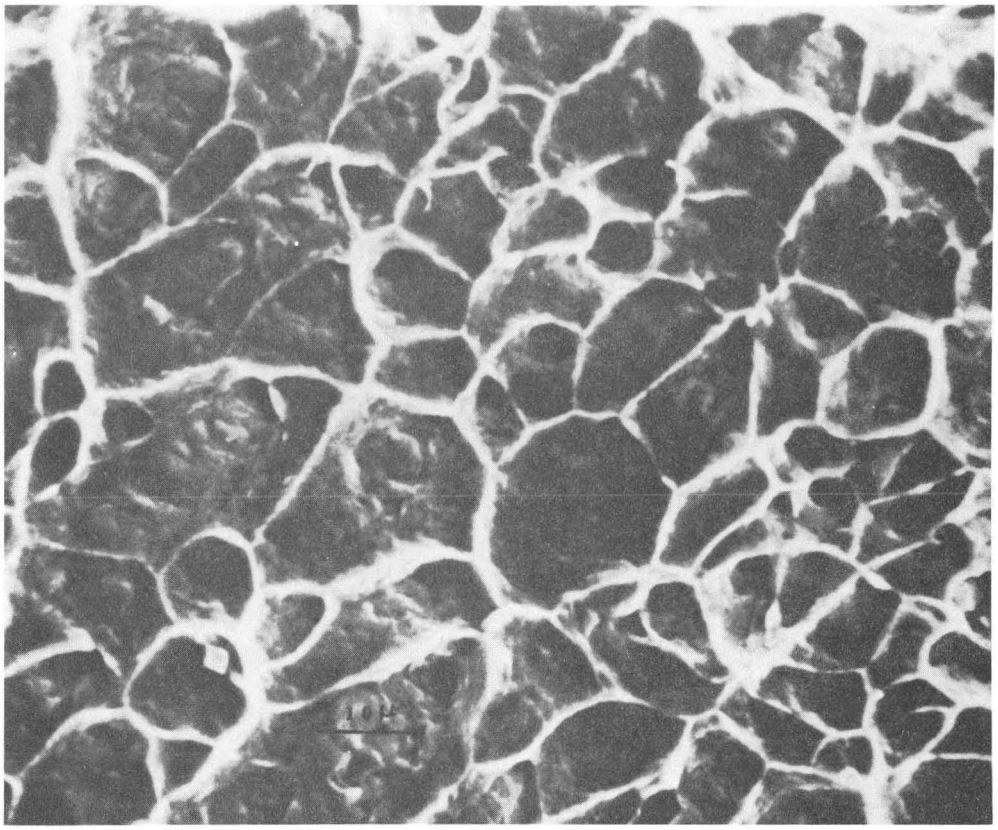

XBB 704-1563

Fig. 36

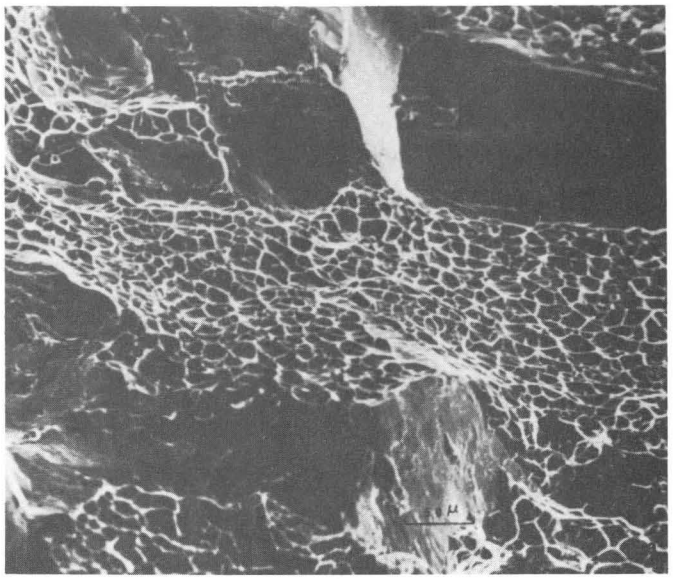

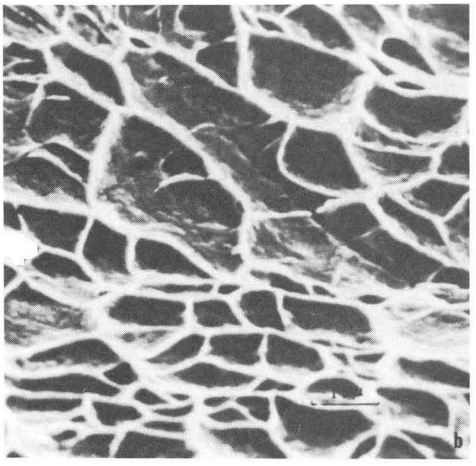

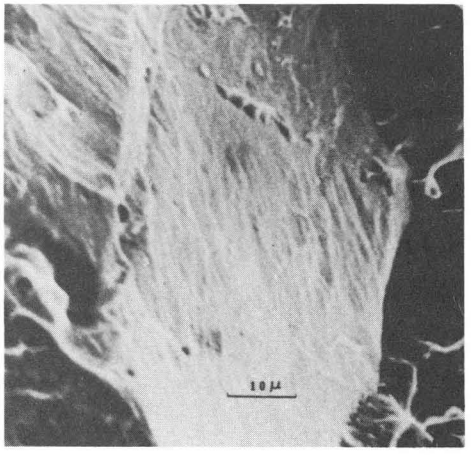

XBB 704-1545

Fig. 37

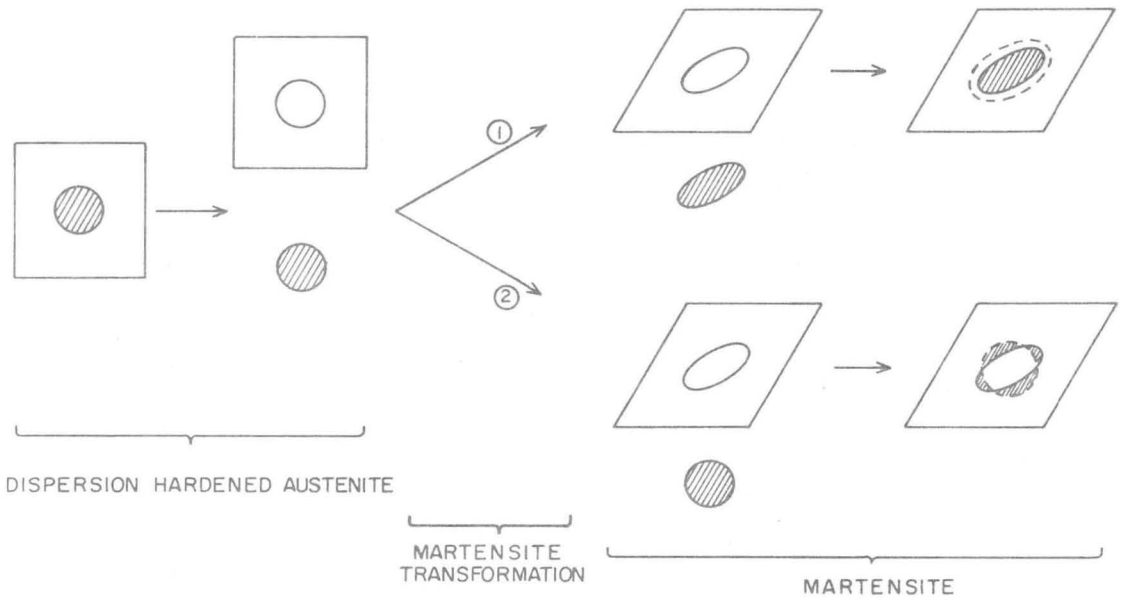

XBL 704-666

Fig. 38

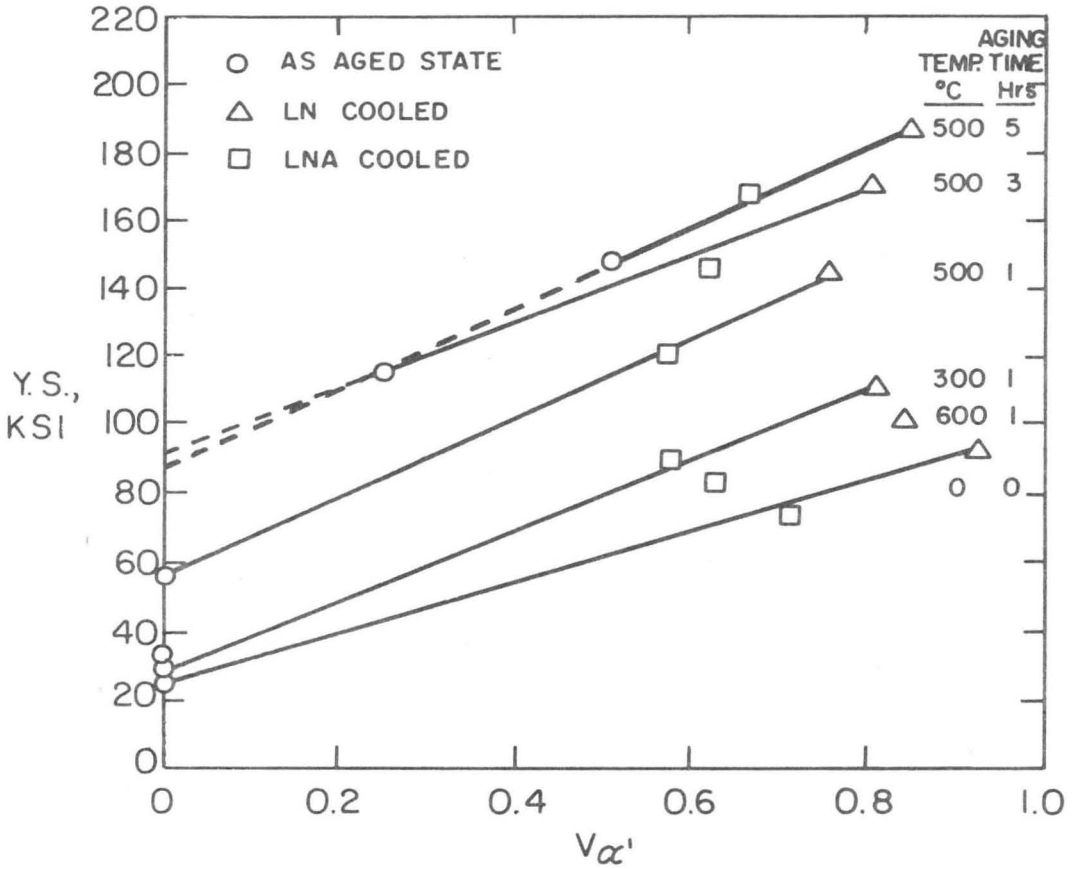

XBL 704-667

Fig. 39

TECHNICAL INFORMATION DIVISION
LAWRENCE RADIATION LABORATORY
UNIVERSITY OF CALIFORNIA
BERKELEY, CALIFORNIA 94720